CHAPTER 3

VEHICLE-TO-GRID INTEGRATION FRAMEWORK

3.1 Introduction

In the previous chapter, the state-of-the-art of microgrid integration systems with various energy sources has been presented. Choosing reliable sources for producing electricity is the base needed for any community to improve living standards and cost-effectiveness to evaluate microgrid systems. The Energy Management Strategies (EMS) as a supervisory control method has been presented along with its classification, advantages, and disadvantages. A number of papers on EMS have been investigated in the literature, and Rule-Based EMS is shown to be the most effective method in decision-making. Various nature-inspired optimization algorithms in terms of artificial intelligent methods with the objective function followed by constraints were highlighted. The technology of Vehicle-to-Grid (V2G) fundamental terminology has been defined with the applicable integrated Renewable Energy Sources (RESs), and the topologies and the impacts were discussed. Consequently, the research gap of the study has been closed in the chapter summary after a critical review of the literature. The proposed system for this study uses a grid-connected system considering a residential load area integrated with RESs and batteries to charge and discharge the EVs is discussed in this chapter.

This chapter presents the systematic methodology for achieving the objective functions of this study along with the proposed algorithm namely Improved Antlion Optimization (IALO) as shown in Figure 3.1. The chapter also presents an explanation of the case study with the proposed system along with mathematical models for system components. Similarly, RB-EMS accompanied by its constrain has been presented to meet the study's objective functions. The proposed IALO algorithm is compared with Antlion Optimization (ALO), Particle Swarm Optimization (PSO), and Cuckoo Search Algorithm (CSA) are presented. Moreover, estimating and analyzing the uncertain

number of arrival and departure EVs as well as the behavior impact of Electric Vehicles (EVs) on the grid using the Stochastic Monte Carlo Method (SMCM) is illustrated. The systematic approach of presenting the research methodology of the study in order to achieve the objective functions and the result is illustrated in Figure 3.1. Starting with step one of data collection (weather, EV, and load demand) to obtain the anticipated result (data figure will be presented in chapter 4). Followed by step two of choosing the utilized system components (WT, PV, Inverter, and BT) for the proposed model integrated with EV to form the V2G system. Subsequently, the proposed high supervisory control algorithm (RB-EMS) is applied for acquiring optimum results. Then, the proposed sizing method (IALO) complemented the RB-EMS for the microgrid to achieve an economic system and then validated it with other utilized methods. Finally, the results obtained from IALO will be analyzed to gain the estimated impact on the grid when integrating an uncertain number of EVs under different scenarios using SMCM. The proposed scenarios (V2G, G2V, RESs2V, BT2V) considered a different number of EVs which are classified as minimum, medium, and maximum EVs (10, 30, and 60), respectively.

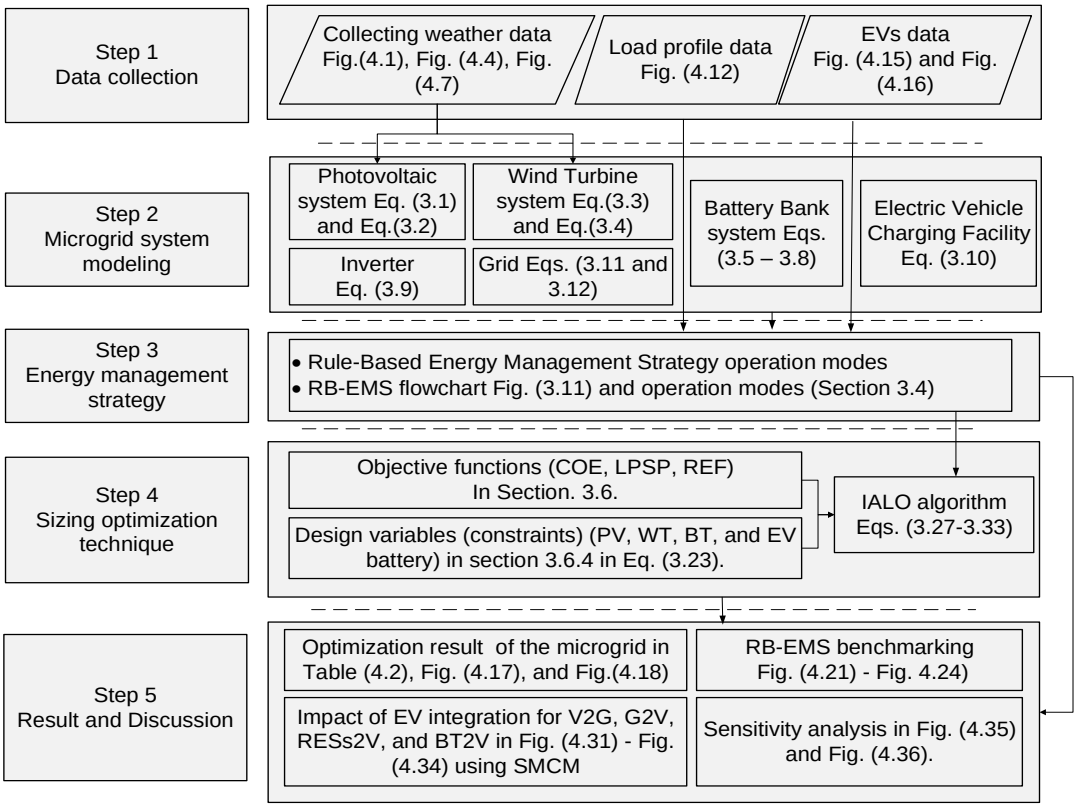

Figure 3.1 A systematic approach for the research methodology and modeling the system and achieving the objectives.

In the first instance, the microgrid test case system is designed using an RB algorithm as integration architecture which is listed below. Subsequently, implementing the proposed optimization method (IALO) for sizing the microgrid components, was then compared with ALO, PSO, and CSA. The process of using RB-EMS and metaheuristic algorithms is a reasonable integration to meet the objective functions [56].

- Evaluation of climatology data (Solar irradiance (W/m^2), Wind Speed (m/s), Ambient temperature (°C), and check the load profile for the grid.

- Structural components of the system.

- Mathematically model the system components.

- Design and simulate the Energy Management strategy of the system.

- Sizing the components system by IALO then compared with ALO, PSO, and CSA.

3.2 The Case Study

Libya is located in the center of North African countries and has high horizontal solar irradiance which reaches up to 7.1 and 8.1 kWh/m^2/day in the coastal and southern regions, respectively [165]. The population is around 6 million people spreading on land out over 1750,000 km^2 [166]. The considered location in this study is located in the north-west region of Libya (Tripoli) with coordinates: 32.8872° N latitude and 13.1913° E longitude [7]. Tripoli's area, inhabitants, and sea-level evaluation are 1507 km^2, 3 million, and 21 m, respectively [167]. The climatic conditions of Libya are influenced by the Mediterranean Sea to the north and the Sahara to the south under four seasons [7]. The average duration of sunlight in Libya is more than 3000 h/year according to a provided report from the Libyan Renewable Energy Authority (LREA) [165]. Besides, wind speed has a high average in the

country as reported in [166] is 7.5 m/s in Derna, 6.6 m/s in Misrata, and 6.5 m/s in Tripoli, respectively [7]. In addition, the direct normal irradiance for the studied area is shown in Figure 3.3.

The main sources of energy in Libya are fossil fuel-based (oil and natural gas) [7]. However, due to the rapidly increasing population in the country, electricity requirements have increased as demonstrated in Figure 3.2. The increase in population causes an increase in electricity demand and environmental problems in the country. Due to the foregoing reason, scholars are trying to utilize the alternative resources that are available in the country such as wind and PV to combat the energy crisis. General Electricity Company of Libya (GECOL) is the only company distributing electricity (administrated) in the country [168]. According to a provided study by the world bank, almost 99.8 % of the citizens had access to electricity as it is the driver of any economy [169]. Libya likes other countries in the world suffered from rapid demand growth, environmental issues, and high energy consumption. Moreover, the issues and usage including energy production, distribution, and consumption are considered [170].

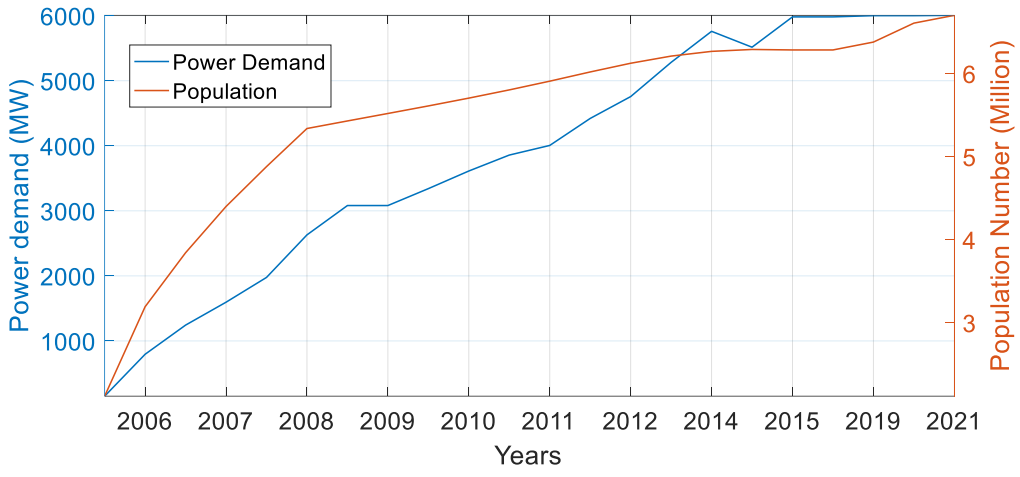

Figure 3.2 The peak load growth in Libya from 2010 to 2021 [7], [167].

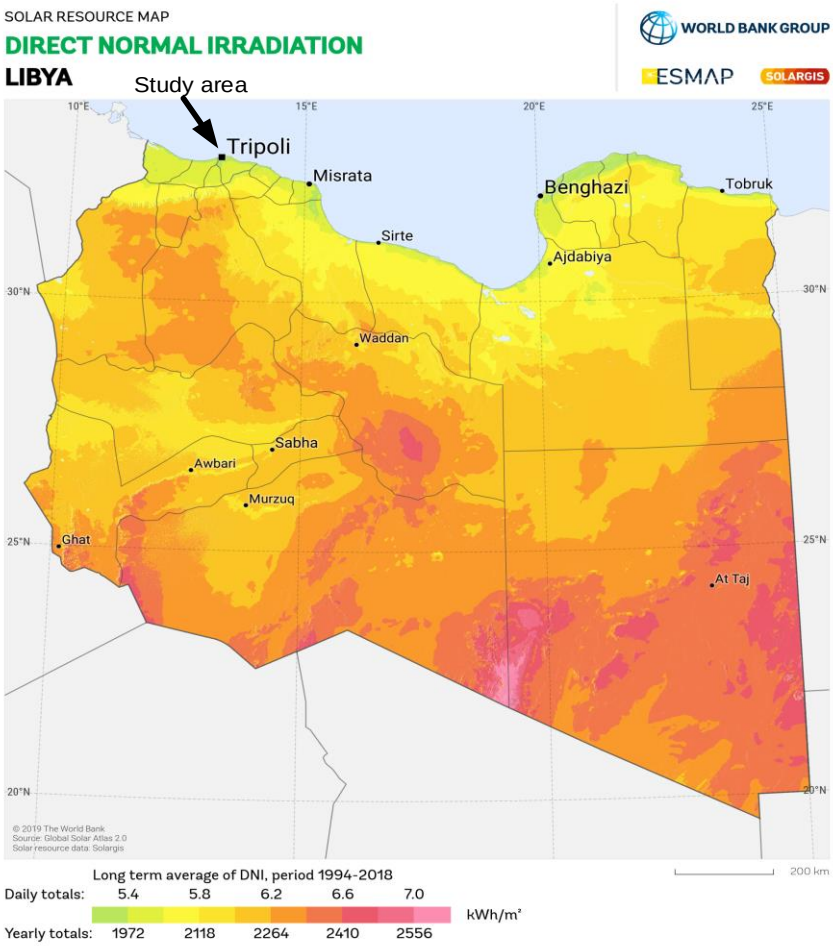

Figure 3.3 Direct normal irradiance for Libyan map [171].

The reason for considering the energy policy in this study is to present how the government or organizations plan and address the growth in energy [7]. The status planning of energy generation in Libya is shown in Figure 3.4 [167]. The energy policy of the country is utilizing crude oil and natural gas as the main essence of the economy as demonstrated in Figure 3.5 (a) with the exported oil and gas to different countries shown in Figure 3.5 (b), respectively [167].

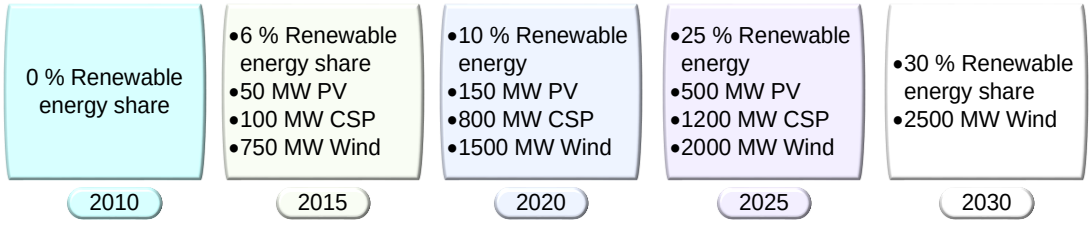

Figure 3.4 Energy plan for the study area [167].

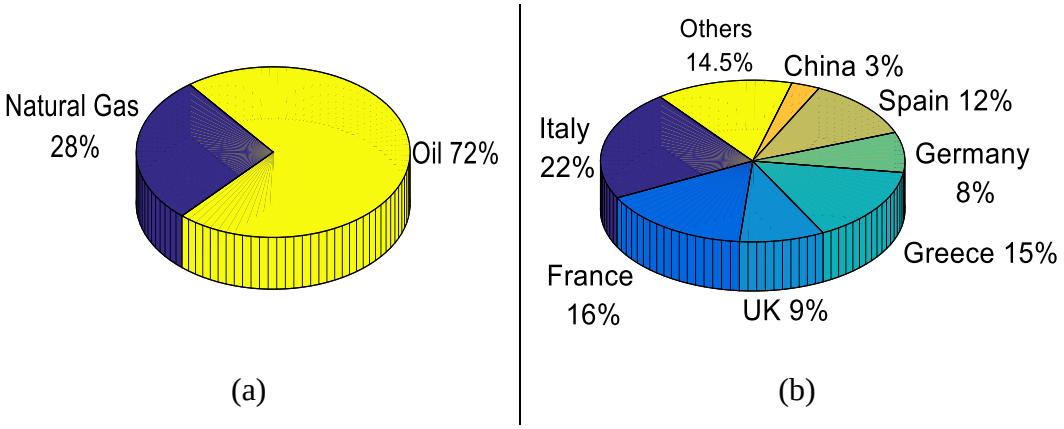

Figure 3.5 Non-renewable sources in Libya (a) Total energy consumption and (b) Crude oil exports to other countries [167].

The country is rich in natural sources such as gold, oil, and the sun. Libya ranked as the fourth country in Africa as an oil producer as the main source of economic [167]. However, due to the increasing environmental issues globally and climate changes, the United Nations (UN) are treating the aforementioned issues by utilizing the available RESs to reduce Carbon Dioxide (CO_2) and Greenhouse Gas (GHG) emissions by 80 % by 2050 [166]. In terms of fuel, the power stations in the country depend on light and heavy oil, and natural gas as percentages are presented in Figure 3.6 [167].

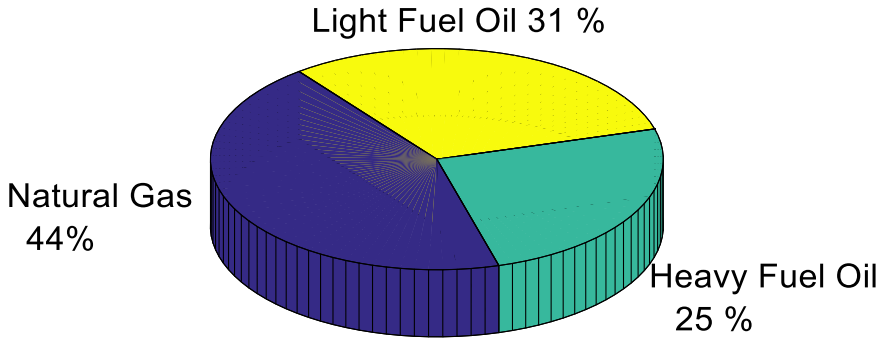

Figure 3.6 Types and percentage of the fuel used in electricity generation [167].

The country is signed several agreements over many years as a member of various organizations to achieve Sustainable Development Goal Seven (SDG7). Libya is a member of the Organization of Petroleum Exporting Countries (OPEC), the agreement was signed in the 1992 Rio declaration (Brazil). In addition, in 1997 Kyoto

Protocol (Japan), and in 2009 Copenhagen (Denmark), respectively [166]. A Libyan organization and planning strategies working in energy and water sectors are National Energy Council of Libya (NECL) and it belongs which are GECOL, Renewable Energy Authority of Libya (REAOL), Libya Atomic Energy Corporation (LAEC), National Oil Committee (NOC), and Ground Water Authority (GWA) [165].

The establishment of the solar system in Libya started in 1976 while the wind system in 2004 [172]. The latter examined the potential of wind speed which was around 6-7.5 m/s at a height of 40 meters. The utilization of PV in lighting and rural electrification in 2003 and water pumping in 1984 [165]. Some solar companies started promoting and installing alternative resources in residential and commercial areas due to the interruption in electricity using PV [166]. Depending on the climate changes for the mentioned location, the four seasons of the year are presented in Figure 3.7 [167].

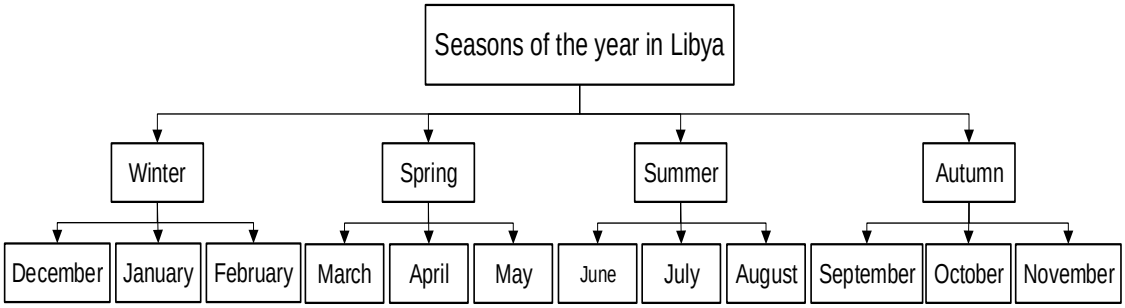

Figure 3.7 Seasons of the year in Libya.

3.3 **The proposed microgrid**

Many studies focus on the design, optimization, and scheduling operation of microgrids [3]. The illustrated system in Figure 3.8 is considered a hybrid DC/AC system with RESs (PV and WT), BT, and residential AC load as the EVCF to form a V2G to charge and discharge a number of EVs. Energy issues and air pollution are two reasons for choosing green sources [116]. The use of RESs to charge EVs in form of RESs2V technology is a challenge because of the few articles that introduced this technique and the intermittency in the weather [18]. The proposed system utilizes two RESs (PV and WT) to generate green energy which has accessibility to the grid.

The management of the battery for charge/discharge of the EV and the system is made through the DC-DC bidirectional converter [20]. Additionally, the generated power from PV used the aforementioned converter for regulating the DC output. Whereas the generated output power from WT passes through the AC-DC converter. During the charging stage, the DC/DC converter functions as a buck converter, and when discharging, it functions as a boost converter [120]. On the other hand, the exploited converter for charging/discharging from the EV is a bidirectional AC-DC that connects with the grid to stabilize the voltage and frequency for a steady-state situation [121].

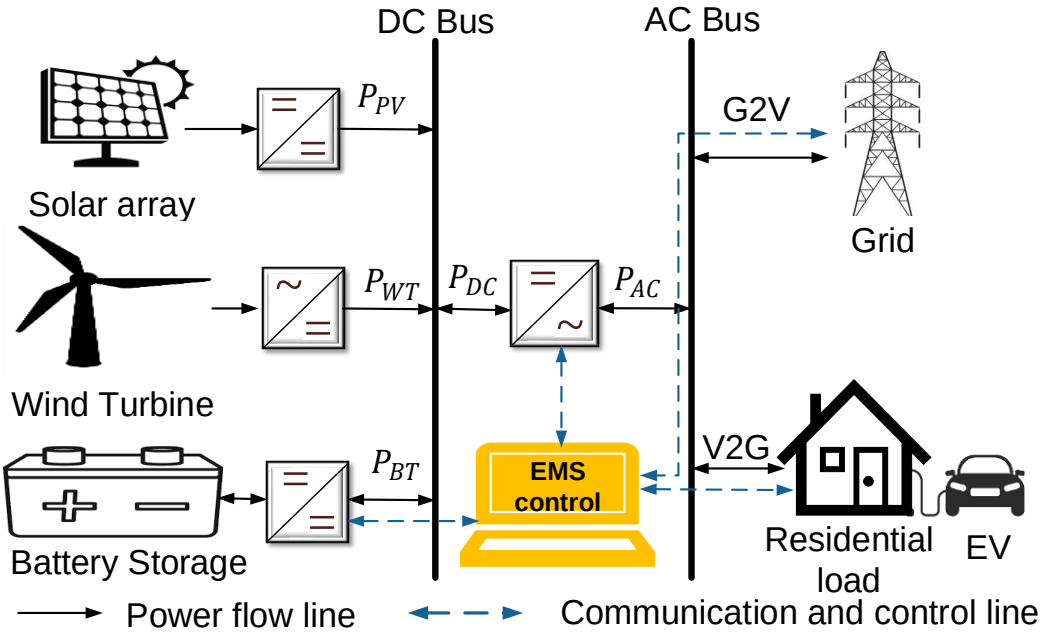

Figure 3.8 The architecture of the proposed Vehicle-to-Grid microgrid.

The working operation steps to meet the proposed objectives in different modes of the microgrid as an EMS using RB-EMS as presented in Figure 3.9. The presented flowchart in Figure 3.9 (a) and (b) is a graphical representation of an RB-EMS algorithm, to simulate the RB-EMS algorithm for the proposed system as listed in Table 3.1. Furthermore, RB-EMS was planned to make a decision since it depends on human knowledge when to sell/buy/store from the utilized sources. Furthermore, no prior data is necessary, and there are no difficult mathematical calculations in RB-EMS.

3.4 Operation modes of Rule-Based Energy Management Strategies

The main mechanism of RB-EMS depends on the (*if* and *then*) statement in the form of operation modes of the system presented in Figure 3.9 and Figure 3.10 for one year of hourly collected data. The first rule refers to Mode 1 considering powering the system from the RESs in case of grid absence as the priority source to meet the renewability function. The second rule is Mode 2 which uses the BT in the case of the absence of the utility grid and RESs are not satisfied. The third one is Mode 3 which depends on the grid to supply the MG system to charge the EV and other appliances which is known as G2V technology. The last rule is Mode 4 which implements the operation of discharging the stored energy from the EV battery (V2G) in case of the absence of the utility grid and not enough supply from RESs and BT. The one-year hourly essential data for the study area as an ambient temperature (T_{amb}), solar irradiance (G), State-of-Charge (SoC), load demand (P_l), EV demand (EV_{dem}), and wind speed (v). Besides, the load profile collected data to produce the output power from PV (P_{PV}) and output power from WT (P_{WT}) are required.

The EMS presented in Figure 3.9 and Figure 3.10 shows the four proposed scenarios that started with the general management diagram of the system presented in Figure 3.9 (a) where the priority is given to RESs to power the system. Where Figure 3.9 (b) represents the discharge operation considering the deep cycle battery (BT) with 20% and 100% as SoC_{min}^{BT} and SoC_{max}^{BT} in the case of not enough energy can be taken from RESs. Figure 3.10 (a) is denoted for charging situations when the absence of RESs or the utility grid supplies the system. Eventually, the operation of utilizing the grid to charge the vehicle (G2V) and utilizing the stored energy in the EV battery to power the home appliances is known as V2G technology is considered in Figure 3.10 (b). The boundaries of SoC_{EV} is considered as $SoC_{EVmin}(0.2\%)$ and SoC_{EVmax} (0.95%), respectively [8].

The presented RB-EMS diagrams in Figure 3.9 (a-b) and Figure 3.10 (a-b) are considering various input data such as P_{PV}, P_{WT}, SOC of BT (E_{BT}), output stored energy of BT in charging mode BT (E_{ch}), and stored energy from BT in discharging mode (E_{dich}). Besides, the maximum output energy of BT (E_{BTmax}), minimum

output energy of BT (E_{BTmin}), the EV demand (EV_{dem}), the utility grid demand ($Grid_{dem}$), and the output energy of the EV (E_{EV}). The working principle of the presented diagrams as shown in Figure 3.9 is measuring the climatology conditions for the case study under four seasons. Then, calculating the output power from the RESs (P_{PV} and P_{WT}) and check the average load demand. Based on the *if* and *then* statement, the strategy is begun to implement the proposed strategy modes from Mode 1 – Mode 4. Furthermore, from the result decision of the *if* and *then* statement, the discharging (A) and charging (B) situations are obtained. The simulation confirmed through the initial SOC of BT, PV-rated power (5kW), WT-rated power (5kW), and BT-rated capacity 35.38 kWh is used as RB-EMS input data. The other presented cases in Figure 3.10 (a) are referring to (B) with the consideration of BT and (C) in Figure 3.10 (b) refer to the operation of charging (G2V) and discharging (V2G).

The four proposed operation modes are listed below along with *if-then* operations as tabulated in Table 3.1 that implement in the flowchart in Figure 3.9 and Figure 3.10 with further explanation shown in Figure 3.11 using software implementation only. If the EV charging/discharging is properly managed, the load demand will be decreased during peak hours which means the overloading will not be acquired.

1. Receiving power from RESs (PV and WT) for running the system by charging BT and charging EVs battery.

2. Receiving power from the battery in case of the absents of the grid and low RESs and charging EV.

3. Receiving the power from the main grid (buying-charging-G2V) when EV demand is high and the absence of RESs and BT. This process is known as unidirectional power flow.

4. Receiving the power from the EV (V2G-sell-discharging) when grid demand is high with the absence of RESs and BT. This process is known as bidirectional power flow.

Table 3.1 RB-EMS rules for a grid-connected system with V2G technology.

Rule No.	Modes	IF (condition)	THEN (operation)
1	RESs	$P_{PV}(t) + P_{WT}(t) > P_l(t)$	$P_{PV}(t) + P_{WT}(t)\ to\ P_l(t)\ and\ EV(t)$
2	Discharge (BT)	$P_b(t) > [P_{WT}(t) + P_{PV}(t) - P_l(t)] * \eta_{inv}$	$P_b(t) > [P_{WT}(t) + P_{PV}(t) - P_l(t)] * \eta_{inv}\ to\ P_l(t)\ and\ EV(t)$
3	Charge (G2V)	$Grid_{dem} < EV_{dem}$	$Grid_{dem} < EV_{dem}\ to\ EV$ (G2V)
4	Discharge (V2G)	$Grid_{dem} > EV_{dem}$	$Grid_{dem} > EV_{dem}\ to\ grid\ (V2G)$

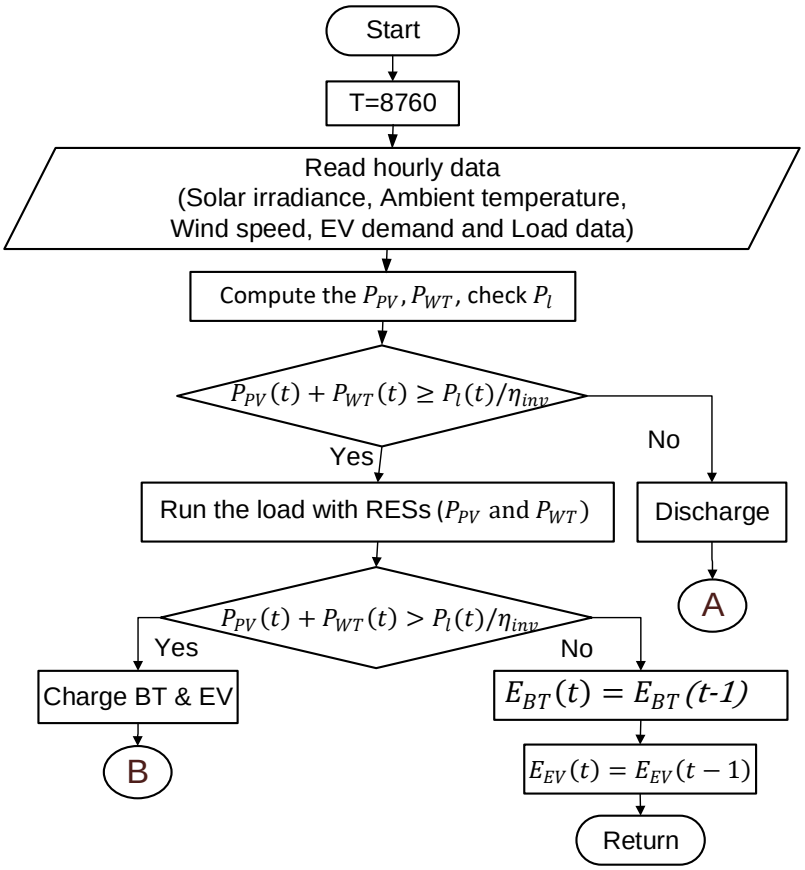

(a)

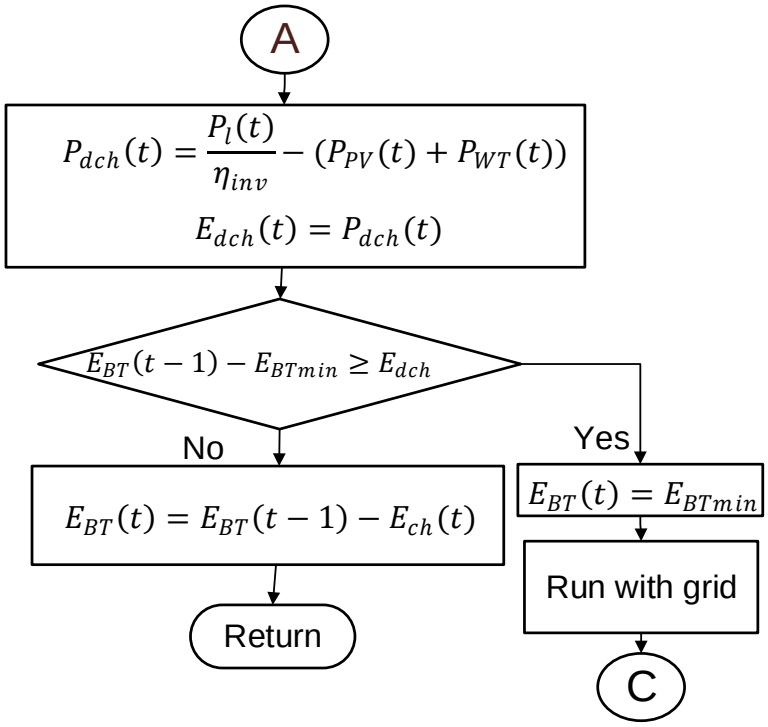

(b)

Figure 3.9 The RB-EMS implementation on the microgrid system (a) The RB-EMS flowchart of the system and (b) Discharging operation from BT.

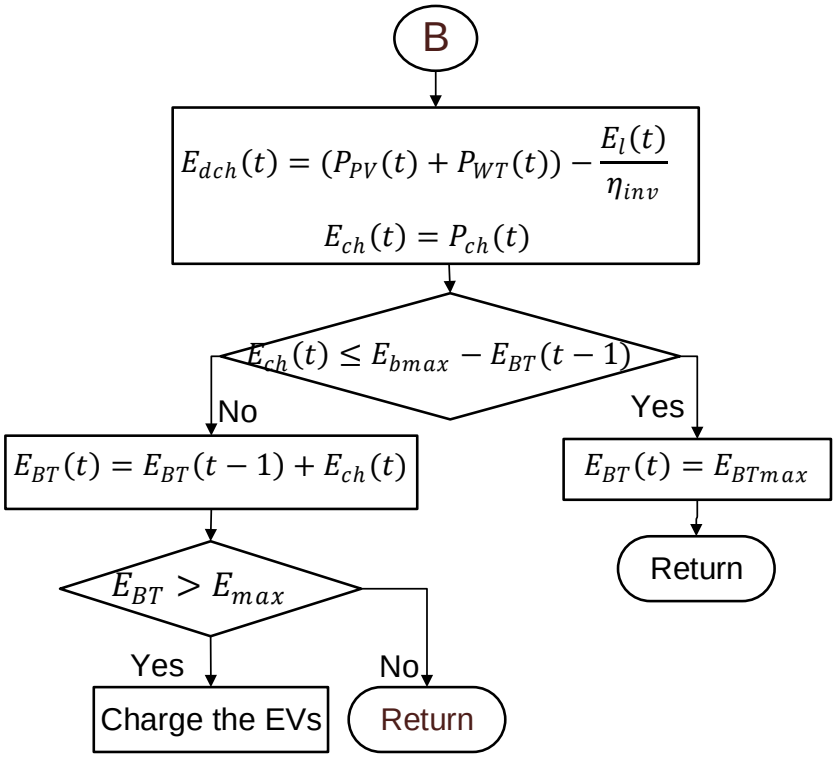

(a)

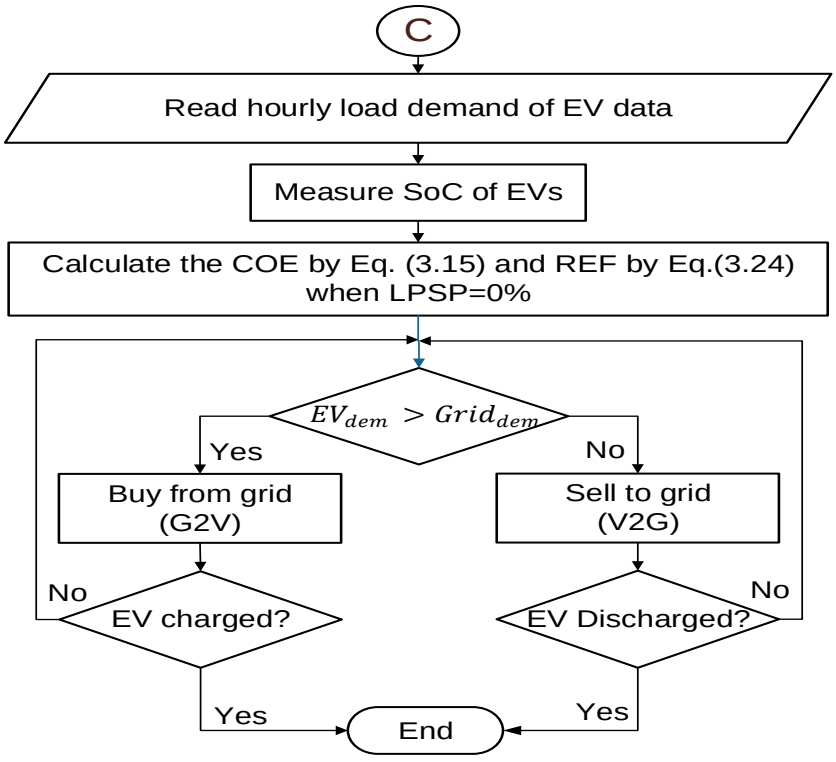

(b)

Figure 3.10 The RB-EMS charging and discharging operation (a) Charging from BT and (b) Buying from the grid (G2V operation) and Selling to the grid (V2G operation).

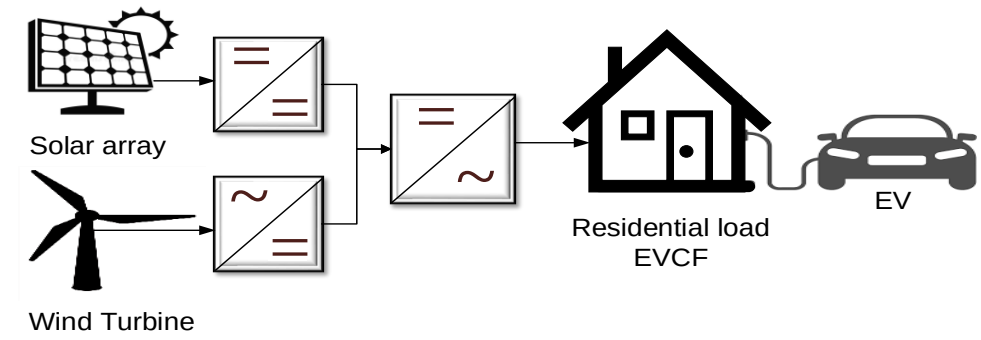

(a)

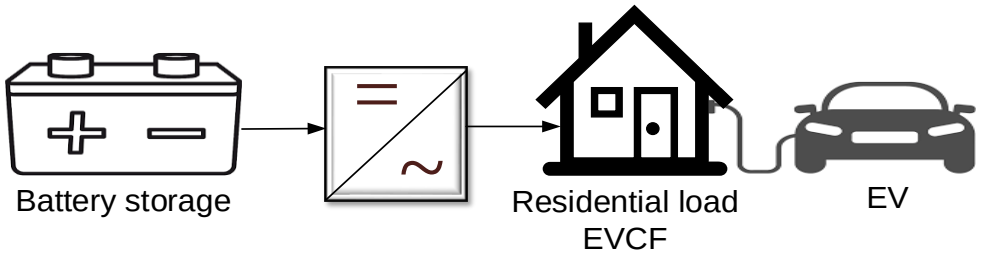

(b)

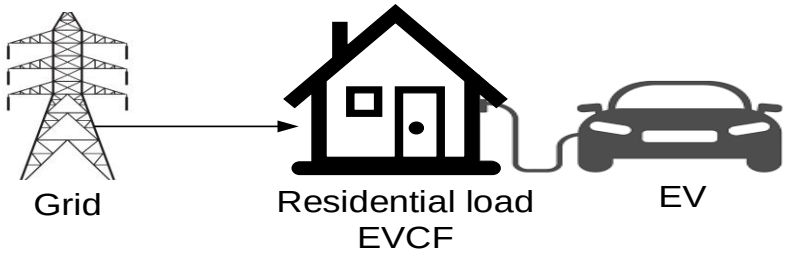

(c)

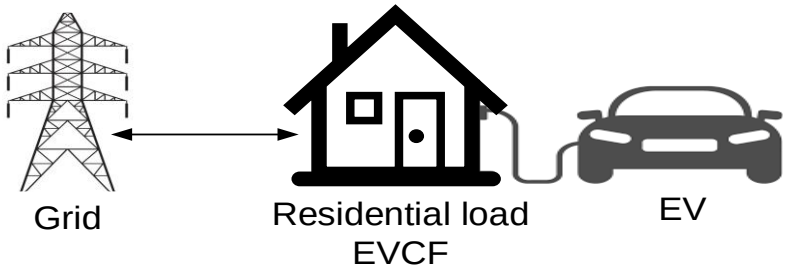

(d)

Figure 3.11 Operation modes of the proposed system. (a) Renewable Energy Sources, (b) Deep Cycle Battery units, (c) Grid-to-Vehicle, and (d) Vehicle-to-Grid**.**

3.5 The Models of the proposed Microgrid Components

Modeling can be defined as the process of identifying objectives, variables, and constraints for a given problem [173]. Many articles have concentrated on

mathematical models for the grid-connected system using V2G technology integration with RESs as an economically-beneficial system [15][46]. Models of the RESs are implemented in this study using MATLAB as a modern software tool to simulate the result of hybrid system components under residential load. The foremost problem with EV drivers is the growing driving range anxiety which means EVCS is required.

Some studies consider PV-EVs integrated with the grid for charging and discharging the EVs [27]. While others hybridize PV and WT at maximum power, and the battery is supporting the system as storage to improve the reliability of the charging station [8], [9]. Designing such a system consists of the presented RESs, sizing is needed and can be presented in [9], [59]. The mathematical model implementation of each component equation will be presented in the next subsections consisting of PV, WT, BT, converter, EVCF, and grid models. The utilized mathematical model equations are widely used among scholars due to their simplicity and cover all the system components [21]. They show the result of reducing the impact of EV demand expansion on the grid [174].

3.5.1 Photovoltaic Model

The most used RESs for producing electricity based on the conversion process from sunlight to produce electricity is PV. The model equation for obtaining the estimated output power generated from the PV system is reported in [158] and presented in Eq.(3.1), while total P_{PV} obtained by multiplying the P_{PV} with N_{PV} at time (t).

$$P_{PV}(t) = P_{(PV_{rated})} \times \frac{G_{(t)}}{1000} * \left[1 + \alpha_t\left(T_C - T_{C_{STC}}\right)\right] \tag{3.1}$$

where $P_{PV}(t)$ is the output power generated from PV in (Watt), $G_{(t)}$ refers to hourly solar irradiance data in (W/m^2) [158], 1000 W/m^2 is the rated radiation at the earth's surface, $P_{(PV_{rated})}$ denotes as rated power for PV in (Watt), $T_{C_{STC}}$ is cell temperature at Standard Test Condition (STC), α_t is the temperature coefficient of the panels that

equls to -3.7×10^{-3} (1/°C) [158]. Additionally, the T_C is the cell temperature in (°C) which can be obtained by Eq.(3.2) [59].

$$T_C = T_{amb} + G_{(t)} \times \left(\frac{NOCT - 20}{800}\right) = T_{amb} + G_{(t)} \times (0.03125) \tag{3.2}$$

The T_{amb} is the ambient temperature (°C) that uses time-series data. Besides, the value of 0.03125 °C was obtained by subtracting the value of Nominal Operation Cell Temperature (NOCT) from air temperature equal to 20 °C. The considered NOCT is 45 °C in this study depending on the PV module specified by the manufacturer. The acquired result is divided by the irradiance on the cell surface (800 W/m^2) to get 0.03125 °C [175].

3.5.2 Wind Turbine Model

The second mentioned type of RESs is the most commonly used due to its advantages such as the ability to collect the maximum amount of wind energy for the time of the day. Besides, the ability to adjust the blades' pitch angle to avoid high windstorms. The aforementioned benefits are related to the considered Canadian WT in this study which is Eocycle EO20 with three blades as presented in Table 3.3 [176]. Due to the environmental and economic acquired benefits of using WT as an alternative power generator, WT is exploited. The model equation is presented in Eq. (3.3) for obtaining the generated output power from WT [39].

$$P_{WT}(t) = \begin{cases} 0 & v(t) \leq v_{cut-in} \text{ or } v \geq v_{cut-out} \\ P_r \dfrac{v(t) - v_{cut-in}}{v_r - v_{cut-out}} & v_{cut-in} < v < v_r \\ P_r & v_r < v(t) < v_{cut-out} \end{cases} \tag{3.3}$$

where v_{cut-in} is the cut-in speed and it is very low, $v_{cut-out}$ is the high cut-out, P_r is rated power in (W). The v_r is rated wind speed (m/s) and P_{WT} refers to the output power generated from WT in (kW) with the help of hourly wind speed data (v), where the total power produced from WT can be acquired by multiplying P_{WT} with N_{WT} at a

time (t). Besides, its hub height (h) is the relationship between height from the surface and wind speed that can be calculated in Eq. (3.4) [59].

$$v = v_{ref} \times \left(\frac{\mathrm{h}}{\mathrm{h_{ref}}}\right)^{\gamma} \tag{3.4}$$

where v and v_{ref} are the rate turbine speed and wind speed in (m/s) that recorded at $\mathrm{h_{ref}}$ which refers to the reference height anemometer 43.6 m, h is the hub height that is equal to 30 m, and γ represents the status of the landscape where the turbine is going to be installed within the range [0.1, 0.25] [177]. Furthermore, the γ varies from location to location depending on the topology surface of the utilized area, where 0.1 refer to the flat area and 0.25 non-flat. The ideal power curve and operation region are illustrated in Figure 3.12.

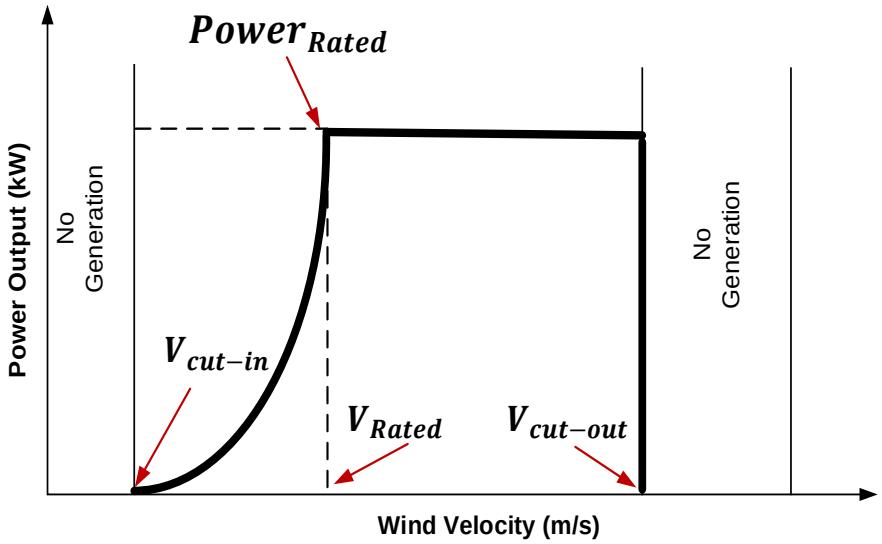

Figure 3.12 The ideal power curve of wind turbines and operation regions [158], [178].

3.5.3 Battery Model

As the backup system of the microgrid in case of sun absences, cloudy days, and issue connection to the main grid or RESs, the battery is used. The mathematical

model of computing the battery capacity can be acquired by using Eq. (3.5). The utilized deep cycle battery is Li-Ion with its datasheet reported in [140], [158].

$$C_B = \frac{P_l \times AD}{DOD \times \eta_{inv} \times \eta_b} \tag{3.5}$$

where C_B is the capacity of the battery in (Ah), P_l is the daily average load demand in (kW), AD is the autonomy days (typically 3-5 days). The DoD is the Depth-of-Discharge (80%), η_b is the battery's efficiencies (85%), and η_{inv} is the inverter's efficiency (95%) [95]. Eq. (3.6) is used to calculate the power delivered from the battery in the case of utilizing RESs only [179].

$$P_{BT}(t) = \left(P_{PV}(t) + P_{WT}(t)\right) - \frac{P_l(t)}{\eta_{inv}} \tag{3.6}$$

where $P_{BT}(t)$ is the power delivered from the battery and $P_l(t)$ is the total energy demand. Calculating the SoC (t) of the battery while charging or discharging can be calculated by Eq. (3.7) and Eq. (3.8), respectively [69]. The limitation of the SoC is used to determine the quantity of charge in the battery at a time (t).

$$SoC(t) = SoC(t-1).(1-\sigma) + \left(\left(P_{PV}(t) + P_{WT}(t)\right) - \frac{P_l(t)}{\eta_{inv}}\right) \times \eta_b \tag{3.7}$$

where σ is the self-discharge rate of the battery equals 0.007% hour [59] and the $SoC(t)$ denotes as the state-of-charge of the battery at a time (t) [158]. The discharging of the battery can be presented by Eq. (3.8).

$$SoC(t) = SoC(t-1).(1-\sigma) + \left(\frac{P_l(t)}{\eta_{inv}} - (P_{PV}(t) + P_{WT}(t))\right) \times \eta_b \tag{3.8}$$

The battery is set to operate at an SoC ranging from 20 to 100% which can be expressed as $SoC_{min}^{BT} \leq \mathrm{SoC}^{BT} \leq SoC_{max}^{BT}$. The DoD presents the percentage of charge consumed in a battery is dependent on battery life with the temperature. While the SoC presents

the remaining charge in the battery as illustrated in Figure 3.13 the essential concept of battery. This storage can be recharged depending on manufacturer specifications [138], [139]. Table 3.2 presents the specification of $LiFePO_4$ as the mostly utilized battery.

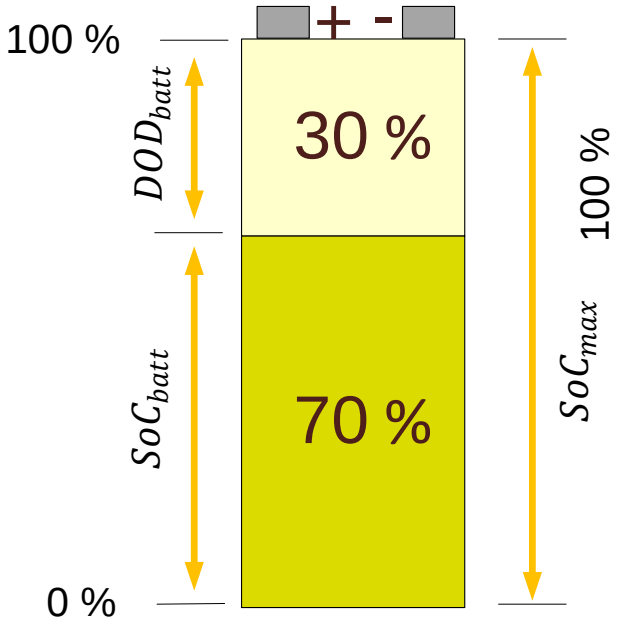

Figure 3.13 The essential concept of battery SoC and DoD.

Table 3.2 Specification of EV ($LiFePO_4$) battery [140], [141].

Parameters	$LiFePO_4$	Units
Nominal voltage	3.2	V
Energy density	120	Wh/Kg
The volumetric energy density	220	Wh/L
Specific power	2000-4500	W/kg
Life cycle	>2000	-
Operating temperature	-45 to +70	1C
Production cost	350	$/kWh
Efficiency	99	%
Initial Temperature	20	^{o}C
Discharge power	1200	W

3.5.4 Converters Model

To convert the power in the system from DC to AC, a converter is required. They play the role of either rectifier (AC/DC) or inverter (DC/AC) which allows the power transfer between the sources and end-user. The inverter efficiency (η_{inv}) is 95% and the output convergence power ($P_{inv}\ output$) at the time (t) can be calculated using Eq. (3.9) [59].

$$P_{inv}\ output(t) = (P_{PV}(t) + P_{WT}(t)) \times \eta_{inv} \tag{3.9}$$

3.5.5 Electric Vehicle Charging Facility model

The EVCF is a utilized area for charging EVs to continue driving and reduce the anxiety of drivers. The amount of EV power demand can be estimated by Eq. (3.10) [69].

$$P_{EV_{Dem}} = \frac{C_{\text{bat}}^{\text{EV}} \times \left(\text{SOC}_{max}^{\text{EV}} - SOC_{\text{min}}^{\text{EV}}\right)}{\text{T}} \tag{3.10}$$

where the $P_{EV_{Dem}}$ represents the EV power demand in (kW), $C_{\text{bat}}^{\text{EV}}$ is the EV capacity which is 14 Ah that is considered in this study [8]. The SOC_{EV} is randomely built in the range of 0.2% and 0.95% as ($SoC_{min}^{EV} \leq SoC^{EV} \leq SoC_{max}^{EV}$) using one of the stochastic methods namely normal distribution in range of [0,1] [180], and T indicates the difference between the arrival and departure times $\left(T = T_{\text{arrive}}^{\text{EV}} - T_{Dep}^{EV}\right)$ [69].

3.5.6 Utility Grid Model

The main purpose of EVCF is to continuously supply the load with the needed power of EV. During the absence of `RESs energy and the battery is not charged, the system can be supplied from the main grid. To count the amount of purchased energy in (kWh) from the grid $\left(P_{\text{P}}^{\text{grid}}\right)$ to the EV which presents (G2V) can be calculated

using Eq. (3.11) [69], while the amount of sold energy from the EV to the grid $\left(P_{\mathrm{S}}^{\mathrm{grid}}\right)$ is calculated using Eq. (3.12) [21].

$$P_{\mathrm{P}}^{\mathrm{grid}}(\mathrm{t}) = P_{EV_{Dem}}(\mathrm{t}) - [\mathrm{P_{PV}}(\mathrm{t}) + \mathrm{P_{WT}}(\mathrm{t}) + \left[\left(\mathrm{SOC_{BT}}(\mathrm{t}) - \mathrm{SOC_{BT}^{min}}(\mathrm{t})\right) \times \eta_{\mathrm{inv}}\right]] \tag{3.11}$$

$$P_{S}^{\mathrm{grid}}(\mathrm{t}) = [\mathrm{P_{PV}}(\mathrm{t}) + \mathrm{P_{WT}}(\mathrm{t}) + \left[\left(\mathrm{SOC_{BT}}(\mathrm{t}) - \mathrm{SOC_{BT}^{max}}(\mathrm{t})\right) \times \eta_{\mathrm{inv}}\right]] - P_{EV_{Dem}}(\mathrm{t}) \tag{3.12}$$

To count the revenue (R_{grid}) from selling energy to the grid can be calculated using Eq. (3.13) [181].

$$R_{grid} = \sum_{t=1}^{8760} rate_{feed-in} \times E_{grid(selling)} \tag{3.13}$$

where the $rate_{feed-in}$ refers to the feed-in tariff rate which is (0.05 $/kWh) multiplied with $E_{grid(selling)}$ that indicates the selling energy [181]. While 8760 refers to the number of hours for one year per hour. Additionally, the purchasing cost of the bought energy (C_{grid}) from the grid is calculated using Eq. (3.14) [21].

$$C_{grid} = C_p \times \sum_{t=1}^{8760} E_{grid(purchased)} \tag{3.14}$$

The C_p is the cost of buying 1 kW of electricity from the grid which equals (0.04 $/kWh) in Libya [181], $\sum_{t=1}^{8760} E_{grid(purchased)}$ refers to the summation of buying electricity from the grid for one year [21]. Additionally, the designed variables (control parameters) are listed for the utilized components of the microgrid and are tabulated in Table 3.3 including the PV-WT-BT-EVCF-grid-converter-economic parameters.

Table 3.3 Summary of the hybrid system components.

Components	Parameters	Value	Unit
PV system [127][175]	Lifetime	25	Years
	Rate Power at STC	325	W
	Operation & Maintenance (O&M) cost	20	$/year
	Initial cost	2.15	$
	Temperature coefficient (α_t)	-3.7×10^{-3}	1/°C
	Replacement cost	0	$/year
	Nominal operating cell temperature	45 ± 2	°C
	Regulator Cost	1500	$
Wind Turbine [176], [179], [181]	Lifetime	25	Years
	Replacement cost	0	$/year
	Cut-in speed (V_{cut-in})	2.8	m/s
	Cut-out speed ($V_{cut-out}$)	20	m/s
	Rate Power of Wind Turbine	1	kW
	Operation & Maintenance (O&M) cost	50	$/year
	Rate Speed (Vr)	7.5	m/s
	Blades diameter	15.8	m
	Hub height (h)	30	m
	Overall efficiency	26	%
Battery Storage [182] [158] [8][140]	Lifetime	10	Years
	Initial SoC of battery	100	%
	$\mathrm{SoC_{min}}$	20	%
	$\mathrm{SoC_{max}}$	100	%
	Minimum charge current	17	A
	Maximum charge current	14	A
	The initial cost of the battery	280	$
	Nominal battery capacity	42	Ah
	Battery capacity	40	Ah
	Replacement cost	280	$/year
	Hourly self-discharge	0.007	%/hour
	O&M cost	5	$/year
	Rate capacity	45.2	kWh
	Maximum DoD	80	%
Electric Grid [181]	Power importing price (sell)	0.05	$/kWh
	Power exporting price (purchase)	0.04	$/kWh
Electric Vehicle Charge Facility [183] [9][127]	Max/Min capacity of EV battery	24/20	A
	SoC_{max}^{EV}	95	%
	SoC_{min}^{EV}	20	%
	EV capacity	14	kWh
	Energy density of the Li-ion battery	118-250	Wh/kg
Converter [126][127] [158][181]	Lifetime	15	Year
	Efficiency (η_{inv})	92	%
	Rate power	1	kW
	Operation & Maintenance (O & M) cost	1	$/year
	Initial cost	2500	$
Economic Parameters	Annual interest rate (i)	3	%
	Project life	25	Years

3.6 Objective Functions Optimization of the proposed microgrids

To be more specific, this study is considering the economic aspects in order to calculate the cost of energy. The study used a grid-connected system in Tripoli city-Libya to achieve and evaluate the proposed objective functions by utilizing the RESs (PV and WT) with BT and EVs forming V2G. The annual investment of the system will be calculated to get a reduction of the Cost of Energy (COE), Losses of Power Supply Probability (LPSP), and maximization of the renewability using the Renewable Energy Fraction (REF) technique, respectively. Additionally, the objective functions of this study are presented in the literature to ensure a reliable power supply at a minimum cost and losses with high renewability [21]. This study proposes a multi-objective function by utilizing the IALO in order to meet the objectives and linearly combined.

3.6.1 Cost of Energy

From an economic point of view, calculating the Cost of Energy (COE) as an objective function is presented in Eq. (3.15) [21] defined as the per capita of electricity [158]. COE is known as an infinite source that provides electricity to a system that applies to run electric appliances [21]. To calculate the COE, the Discounted Cash Flow (DCF) analysis method is applied [184]. Where DCF is utilized to approximate or evaluate the value of capital investment money [21]. The term DCF is a modern economic term and presents the summary that is reflecting the present value of money (cost) of the project lifetime. It is designed to calculate the payback period which means all capital costs (O&M, replacement cost, and installation cost) during the lifetime of the system.

$$COE = \frac{(CRF \times \sum_x NPC_x) + C_{grid-} R_{grid}}{E_{served} + E_{grid-selling}} \tag{3.15}$$

The COE presented in Eq. (3.15) can be obtained with the help of the Capital Recovery Factor (CRF) which is used to calculate the present value of money as presented in Eq. (3.16) [185]. The Net Present Cost (NPC) in ($) includes the costs (O&M, replacement

cost, and installation cost) for x of years that can be computed by Eq. (3.17). The $E_{grid-selling}$ indicates the selling energy, E_{served} is the primary load served in (kWh/year) [21].

$$CRF = \frac{i(1+i)^n}{(1+i)^n - 1} \tag{3.16}$$

where i is the real interest rate in (%), n is the amortization period or (system life period) that is equal to the lifetime of the solar panels (25 years) [95]. The ASC refers to the Total Annualized System Cost ($) [21].

$$NPC(\$) = \frac{ASC}{CRF} \tag{3.17}$$

Calculating the cost of each component in order to obtain the Annualized System Cost (ASC) as presented in the equations from Eq. (3.18)-Eq. (3.22) [179].

$$C_{SOL} = C_{PV}^{INST} + C_{PV}^{REP-C} + C_{PV}^{O\&M} \tag{3.18}$$

$$C_{WT} = C_{WT}^{INST} + C_{WT}^{REP-C} + C_{WT}^{O\&M} \tag{3.19}$$

$$C_{BATT} = C_{BATT}^{INST} + C_{BT}^{REP-C} + C_{BATT}^{O\&M} \tag{3.20}$$

$$C_{INV} = C_{INV}^{INST} + C_{INV}^{REP-C} + C_{INV}^{O\&M} \tag{3.21}$$

where C_{INV}^{INST}, C_{PV}^{INST}, C_{BT}^{INST}, and C_{WT}^{INST} are the installation cost of the inverter (per kW), solar panels (per kW), battery (per unit), and wind turbine (per kW), respectively. While the $C_{INV}^{O\&M}$, $C_{PV}^{O\&M}$, $C_{BT}^{O\&M}$, and $C_{WT}^{O\&M}$ are the annual operation and maintenance costs of the inverter, solar panels, battery, and wind turbine, respectively. The C_{INV}^{REP-C}, C_{PV}^{REP-C}, C_{BT}^{REP-C}, and C_{WT}^{REP-C} are the replacement cost of the inverter, solar panels, battery, and wind turbine, respectively [127], [179]. The values of the mentioned components are provided in Table 3.3.

$$ASC = F(N_{PV}C_{SOL} + N_{WT}C_{WT} + N_{BT}C_{BT} + P_{INV}C_{INV}) \quad (3.22)$$

where the C_{INV} is the cost of the inverter (per kW), C_{SOL} is the cost of solar panels (per kW), C_{BT} is the cost of the battery (per unit), and the C_{WT} is the cost of a wind turbine (per kW), and the P_{INV} is the rating power of the inverter. F is the obtained value of CRF [127]. Where the values of NPC of the grid as its replacement cost is zero [179].

3.6.2 Losses Power Supply Probability

The second objective function for measuring reliability is using the Losses Power Supply Probability (LPSP) technique that is presented in Eq. (3.23). The LPSP ranges between $(0 \leq LPSP \leq 1)$, where 0 refers to satisfied load and 1 refers to unsatisfied load. It can be defined as the capability of the power system to deliver electricity to consumers in a secure way without power losses [65]. Furthermore, minimizing the LPSP refers to the probability of power supply failure to meet the load demand which can be computed in Eq. (3.23) [9].

$$LPSP(\%) = \frac{\sum_{i=1}^{N}[P_l(t) - \left(P_{PV}(t) + P_{WT}(t) + SoC_{BT}(t) + SoC_{EV}(t)\right)]}{\sum_{i=1}^{N} P_l(t)} \quad (3.23)$$

where the SoC_{BT} denoted as the state-of-charge of a deep cycle battery in a time (t), while the SoC_{EV} is the state-of-charge of the EV battery at a time (t).

3.6.3 Renewable Energy Fraction

The last objective function related to this study is to maximize renewability by exploiting the Renewable Energy Fraction (REF) technique [21]. The REF is defined as the quantity of the energy transferred to the load that is generated from RESs that reduces the NPC and CO_2 emission which can be calculated by Eq. (3.24) [111].

$$REF(\%) = \frac{\sum_{1}^{8760}(P_{PV} + P_{WT}) \times \Delta t}{\sum_{1}^{8760}\left(P_{PV} + P_{WT} + P_{grid_{purchased}}\right) \times \Delta t} \quad (3.24)$$

where the $P_{grid\_purchased}$ is referring to the amount of purchased electricity from the grid for one year [21]. The main three presented objective functions have a trade-off. When the LPSP is minimized, the REF is maximized, and the overall system cost rises, increasing the COE. As a result, the designer has to compromise the three objective functions to achieve the optimal result. Additionally, the minimization of the two aforementioned multiple objective functions with the maximization objective has been linearly combined and implemented in IALO as expressed in Eq. (3.25) [59].

$$wF_1 + (1 - w) \times \gamma \times PF \times F_2 + wF_3 \tag{3.25}$$

where the w is the weighting factor that is generated randomly in the range of (0,1) which is set as zero and progressively increases interval of 0.05 up to 1, F_1, F_2, and F_3 are the COE, LPSP, and REF, respectively. Additionally, the γ is a scaling factor that is set as 1000 [59], PF is the balancing factor for the different units of the utilized objectives.

3.6.4 Constraints in an optimization framework

The mentioned objective functions (COE, LPSP, and REF) are considered to gain a minimum cost and reliability along with high renewability in a grid-connected system. Out of the aforementioned objective functions, LPSP and REF are the constraints due to the climatology conditions and not meeting power demand. Besides, the SoC_{EV} during arrival $\left(SoC_{arrive}^{EV}\right)$ and SoC_{EV} during departure $\left(SoC_{Dep}^{EV}\right)$ are considered as a constraint. The number of WT, SoC, PV, and BT in the hybrid system is known as design variables (decision variables) that are evaluated in this study. The boundary (upper and lower) of the components (N_{WT}, N_{PV}, N_{AD}, and N_{BT}) are ranges between $0 \leq 50$, $0 \leq 100$, $0 \leq 5$, and $0 \leq 100$, respectively. While the limits of the design variables (control parameters) is stated in Eq. (3.26). Regarding the number of EVs, this study proposes three cases when integrating 10, 30, and 60 of EVs respectively, which is proposed for each house to have one EV to form V2G technology (charge/discharge). Furthermore, the integration of the three mentioned cases are referring to each EV connected separately in a single house for power exchange.

$$\begin{cases} N_{WT} & N_{WT}^{min} \le N^{WT} \le N_{WT}^{max} \\ N_{BT} & N_{BT}^{min} \le N^{BT} \le N_{BT}^{max} \\ N_{PV} & N_{PV}^{min} \le N^{PV} \le N_{PV}^{max} \\ N_{AD} & N_{AD}^{min} \le N^{AD} \le N_{AD}^{max} \end{cases} \tag{3.26}$$

3.7 The Test Function Application of the proposed algorithm

This section presents four popular benchmark test functions in order to validate the results of the proposed IALO method [33]. According to [54], there is no agreed-on test function list as presented in the literature [33], [186], [187]. The exploited test functions for unimodal are namely, Sphere (F_1) and Schwefel2.22 (F_2), while for the multimodal are Ackley (F_{10}) and Penalized 2 (F_{13}) as presented in [187] as presented in Table 3.4. The unimodal is a function with one global solution in the research space, while multimodal is a function with many local solutions and one global solution [186]. Due to the aforementioned function makes the allowability for benchmark performance with other metaheuristic algorithms in terms of exploration and avoids the quick achievement of the local optima.

Table 3.4 illustrated the widely used test functions for testing the optimization algorithms due to their provided benchmark results in microgrid applications. The sphere test function is the most implemented test function due to the accurate provided result that has local minimum dimensional ranges between [-100,100]. The Schwefel2 test function is a complex function with many local minima ranges between [-100,100]. Ackley function is formed in a two-dimensional and categorized by a nearly flat outer region and a large hole at the middle center and ranges between [-20, 20]. Eventually, the Penalized 2 test function is presented in two-dimensional form and ranges between [-5,5] and has several local minima.

Table 3.4 Unimodal and multimodal benchmark function [33], [54].

Function	Mathematical expression	Dimension	Range
Unimodal Benchmark Function			
Sphere Function (F_1)	$F_1(x) = \sum_{i=1}^{n} x_i^2$	30,200	[-100,100]
Schwefel2.22 Function (F_2)	$F_2(x) = \sum_{i=1}^{n} \lvert x_i \rvert + \prod_{i=1}^{n} \lvert x_i \rvert$	30,200	[-100,100]
Multimodal Benchmark Functions			
Ackley Function (F_{10})	$F_{10}(x) = -20\exp\left(-0.2\sqrt{\frac{1}{n}\sum_{i=1}^{n} x_i^2}\right) - \exp\left(\frac{1}{n}\sum_{i=1}^{n}\cos(2\pi x_i)\right) + 20 + e$	30,200	[-20,20]
Penalized 2 Function (F_{13})	$F_{13}(x) = 0.1\{sin^2(3\pi x_1) + \sum_{i=1}^{n}(x_i-1)^2[1 + sin^2(3\pi x_1 + 1)] + (x_n-1)^2\,[1 + sin^2(2\pi x_n)]\} + \sum_{i}^{n} u(x_i, 5,100,4)$	30,200	[-5,5]

3.8 The Metaheuristic Optimization Algorithms

The proposed algorithm is classified under nature-inspired metaheuristic algorithms, which enable it to overcome microgrid issues [188]. There are numerous methods for solving power flow problems, one of them is Antlion Optimization as presented in the literature with its variations [189]. The main measurement of success or failure of any method is by measuring the time, accuracy, and optimality [6], [20]. The utilized algorithm for sizing the system components has been improved due to the faced limitation in the conventional ALO such as premature convergence and quickly falling in the local optima solution. Whereas the improvements were done to Antlion

Optimization (ALO) namely Improved ALO (IALO) is mathematically presented in Section 3.8.2 and has not been applied to the V2G system in the literature yet.

3.8.1 Antlion Optimization

As the original method has been elaborated with the mathematical equations in the previous chapter. The antlion optimization steps are shown in Table 3.5. Applying RB-EMS-ALO is presented in this section as shown in Figure 3.14 by integrating the data of the parameters, load demand, objective functions (COE, LPSP, and REF) and constraints, and economic and technique data into the original nature-inspired algorithm to form the RE-EMS-ALO.

Table 3.5 Steps of Antlion Optimization.

Steps	Implementing operation
Step 1	• Loading weather database (Solar irradiance, Ambient temperature, Wind speed) is shown in Figures 4.2 (a), Figure 4.5 (a), and Figure 4.8 (a), respectively. • The load demand database is figured in Figure 4.18 (c). • The load economic database for the microgrid components is listed in Table 3.3.
Step 2	• Set the ALO constants. - Population size=5, G=20, Max iteration=100, Search agent=10. • Set constraint. - REF and LPSP. • Set the research space: - lower and upper bounds for N_{PV} [0,100] - lower and upper bounds for N_{WT} [0,50] - lower and upper bounds for N_{AD} [0,3] - lower and upper bounds for N_{BT} [0,100]. • Update the fitness for each ant and antlion. • Select an antlion using Roulette Wheel Selection.
Step 3	• Updating the position between the antlion and elite using Eq. (2.3)
Step 4	• Update the position of all ants. • If updated calculate the fitness for each ant and antlion, if not go to step 2
Step 5	• Search the optimal solution in the antlion group
Step 6	• If the best solution is obtained stop, if not repeat step 2

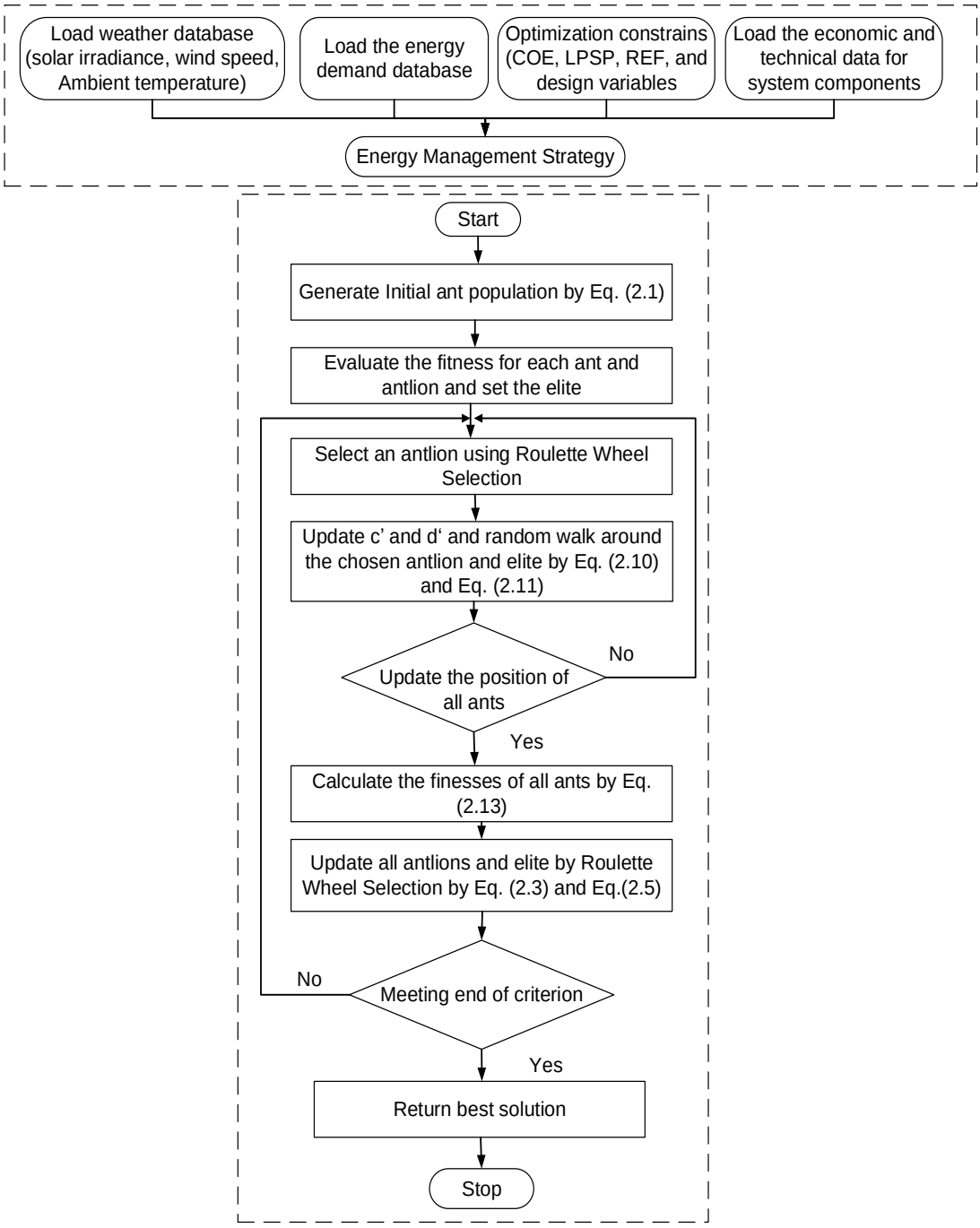

Figure 3.14 Flowchart of Rule-Based Energy Management Strategy of ALO.

3.8.2 The proposed Improved Antlion Optimization

Several metaheuristic algorithms have been improved in the literature through the previous years and applied in various applications. The IALO is one of the developments of the ALO algorithm from the perspective of better accuracy and optimality [190]. Due to the provided merits by ALO, ALO is employed to solve

different optimization problems such as benchmark functions, machine learning, scheduling, and control of power. Besides, smart grid, networking, feature selection, software engineering, and solving the limitation of the ALO method [74]. A challenge that minimizes the size of chosen features and maximizes classification efficiency is known as feature selection [75]. The technique of feature selection involves choosing a meaningful subset of characteristics (selection of individuals in metaheuristic algorithms) from a large set [191]. Where the feature selection classifies into two groups: wrapper-based and filter-based [192]. The former considers machine learning techniques as used in this study. In contrast, the latter considers being computationally inexpensive due to the search for the optimal settings from the vast region of dimensionality [193]. Various feature selections have been projected such as Boltzmann selection, Tournament selection, Roulette Wheel Selection (RWS), Lévy Flight (LF), Linear rank selection, Rough-set, and others [75]. Feature selection can be defined as the process of selecting a significant subset from a huge data.

The differences between ALO and IALO are in the random walk as a selection method as briefly has been elaborated in the previous chapter. Where ALO uses the Roulette Wheel Selection as a feature selection method to choose and update the position of ants and antlions, while IALO uses Lévy Flight [33]. LF is proposed to improve the effectiveness of random walks (local search) in the conventional ALO and is also known as lévy distribution (lévy walk). The LF proposed to address the faced limitations of ALO such as long runtime during the optimization process due to the random movements of the antlion, premature convergence, and quickly falling in the local optima solution. Additionally, RWS is preferable for maximization problems, while LF is utilized with other algorithms for minimization problems as stated in the literature [91]. Both feature selection methods as RWS and LF are used to control the random walk in the proposed algorithm (IALO) and comparison algorithms, however, the latter performs better [33]. Based on the conducted studies, LF has been combined and implemented with other metaheuristic algorithms such as CSA [32], in order to overcome optimization problems in various fields. Additionally, the flowchart of IALO is shown in Figure 3.15, it differs from ALO in updating ant and antlion positions by Eq. (3.27) by applying the LF method as highlighted in action 3. Accordingly, the obtained result from IALO will be benchmarked with the counterparts (ALO, PSO, and CSA) as briefly described in the following subsection.

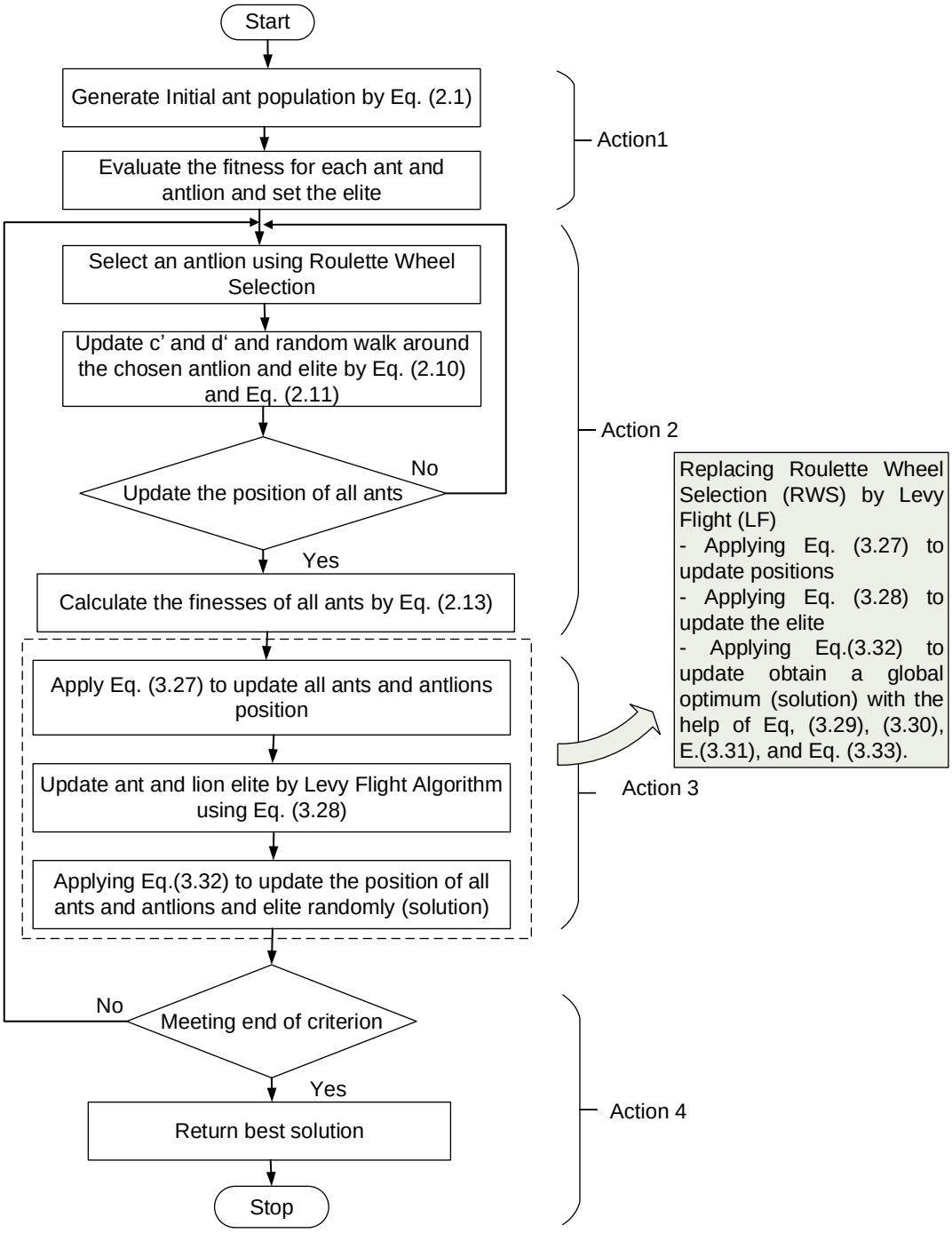

Figure 3.15 Flowchart of the proposed Improved ALO (IALO) Algorithm.

where the improved random walk ($RWX(t)$) can be presented in Eq. (3.27) with the controlled LF that reduces the distance of the random walk.

$$RWX(t) = [0, cumsu(2\mathrm{L}r(t_1) - 1, cumsu(2\mathrm{L}r(t_2) - 1..cumsu(2\mathrm{L}r(t_n) - 1,] \quad (3.27)$$

Furthermore, using lévy flight to improve the search of ALO algorithm and solve microgrid optimization problems for the best number of configurations (elite). Eq. (3.26) was utilized to update all ants and antlions' positions by LF algorithm instead of RWS and Eq. (3.28) updates the new position considering LF.

$$x_i^{(t+1)} = x_i^{(t)} + \alpha_{step} \otimes \text{ lévy } (s) \tag{3.28}$$

where the $x_i^{(t)}$ is the current position of ant, $x_i^{(t+1)}$ denoted as the new position, α_{step} is considered a constant value and known as step size which is considered as greater than 0. s is the step length that can be mathematically expressed as in Eq. (3.29) and $\otimes$ is the entry-wise multiplication (refers to a matrix with the same dimension). Essentially, LF is providing a random walk, where the steps can be drawn by Eq. (3.30).

$$s = \frac{\varphi \times \mu}{|\alpha|^{\gamma}} \tag{3.29}$$

$$\text{lévy } (\gamma) \sim u = t^{-\gamma}, 1 < \gamma \leq 3 \tag{3.30}$$

where α and μ are denoted as the normal distribution (standard deviation and mean) in Eq. (3.30), u refers to the uniformly distributed value [1,3], and γ is lowercase gamma that is greater than 1 and less or equal to 3 ($1< \gamma \leq 3$), it assumed to be 1.5. The φ is called the lowercase of Phi which can be calculated in Eq. (3.31) [75].

$$\varphi = \left[\frac{\Gamma(1+\gamma) \times \sin(\pi \times \gamma/2)}{\Gamma\left(\left(\frac{1+\gamma}{2}\right) \times \gamma \times 2^{\left(\frac{\gamma-1}{2}\right)}\right)} \right]^{1/\gamma} \tag{3.31}$$

The Γ refers to the uppercase standard gamma function that equals $\sqrt{\pi}$, where the uniform distribution random walk ($RaWa$) for both ant' and antlion' is performed in Eq. (3.32).

$$RaWa = \mathrm{Ant}_{\mathrm{i}}^{\mathrm{t}} + \omega \times s \times r \times \left[\mathrm{Antlion}_{\mathrm{j}}^{\mathrm{t}} - \mathrm{Ant}_{\mathrm{i}}^{\mathrm{t}}\right] \tag{3.32}$$

where ω is a controlling scale for the random walk considering the current iteration (t) and the number of allowable iterations (N) that can be mathematically expressed in Eq. (3.33). The subtracting operation is to update the position of antlion and ant.

$$\omega = 1 - \frac{t}{N} \tag{3.33}$$

Furthermore, the mathematical steps for the proposed algorithm are presented in Eq. (3.27) - Eq. (3.33), and further steps are tabulated in Table 3.6 [78], the implementation process of the RB-EMS-IALO is illustrated in Figure 3.16.

Table 3.6 Steps operation of the proposed IALO and its description.

Steps	Implementing operation
Step 1	Randomly initialize the position of ants and antlions as referred to in action 1 in Figure 3.15.
Step 2	Calculate the fitness of the antlions and ant to choose the antlion whose fitness is best as the elite
Step 3	• Select an antlion using the Roulette wheel selection and calculate the random walks around the chosen antlion and the elite. • Update the ants' position with Eq. (2.2) - Eq. (2.9).
Step 4	Repeat step 3 until the positions of all the ants are updated
Step 5	• Update the antlions' positions with Eq. (3.30). • Compare the fitness of the new antlions with the fitness of the elite. • If the antlions have better fitness, then the elite will be replaced by the position of the antlion.
Step 6	Update the position of ants and antlion by lévy using Eq. (3.27) - Eq. (3.33) are adopted to search for better antlions and update the elite.
Step 7	Repeat steps 3 to step 7 until the stop criteria are met.

The aforementioned operation steps presented in Table 3.6 for the proposed method (IALO) are placed in steps 5 and 6, while the beginning and the end of the algorithm are similar to the original ALO. The original ALO considered RWS as a feature selection to update the position of ant and antlion, however, it faces premature convergence and acquiring local optima quickly. For addressing the ALO limitations, IALO is enhanced by replacing LF rather than RWS for the same purpose in order to gain a robustness method and improve the randomness.

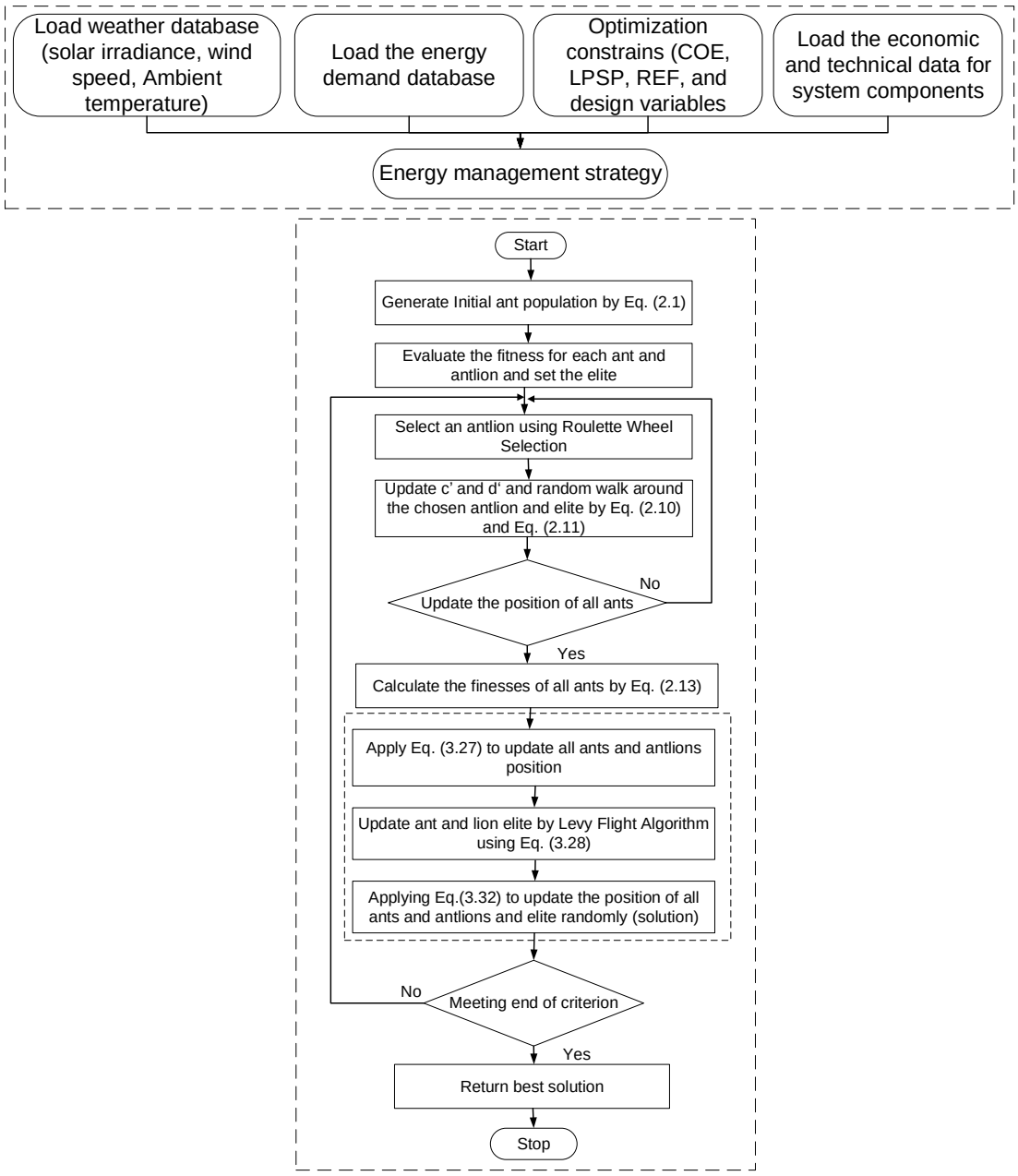

Figure 3.16 Flowchart of the proposed Rule-Based-Energy Management Strategy of IALO (RB-EMS-IALO).

3.9 The benchmark algorithms

The obtained result from the proposed algorithm (IALO) will be validated with other metaheuristic algorithms which are ALO, PSO, and CSA as very well know algorithms. The elaboration for benchmarking utilized algorithms is presented in the subsection below. The benchmarking methods have been chosen as popular methods due to their high efficiency in providing the optimum result. In addition to the complementation of IALO with RB-EMS for the aforesaid methods as RB-EMS-ALO in section (3.8.1), RB-EMS-PSO in section (3.9.1), and RB-EMS-CSA in section (3.9.2) are discussed.

3.9.1 Particle Swarm Optimization

The explanation of PSO has been elaborated in the aforementioned chapter (refer to chapter 2) as a benchmark method for the acquired result from IALO. The flowchart of applying RB-EMS-PSO is presented in Figure 3.17 by inserting load demand, objective functions (COE, LPSP, and REF), and economic and technical data for system components. While the steps of PSO is tabulated in Table 3.7.

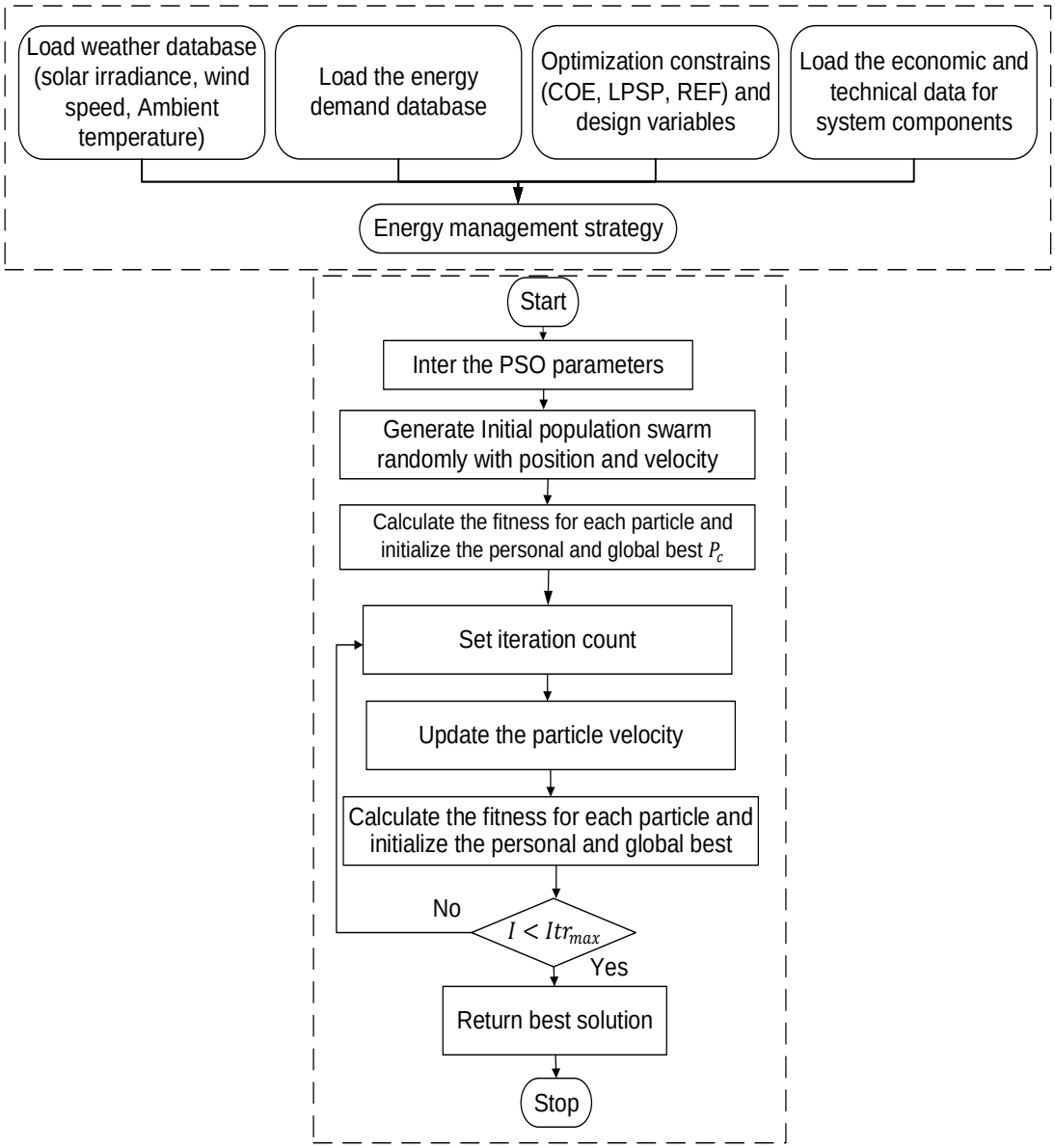

Figure 3.17 Flowchart of the Rule-Based-Energy Management Strategy of Particle Swarm Optimization (RB-EMS-PSO).

Table 3.7 Steps of Particle Swarm Optimization Algorithm.

Steps	Implementing operation
Step 1	• Loading weather database (Solar irradiance, Ambient temperature, Wind speed) is shown in Figures 4.2 (a), Figure 4.5 (a), and Figure 4.8 (a), respectively. • The load demand database is figured in Figure 4.18 (c). • The load economic database for the microgrid components is listed in Table 3.3.
Step 2	• Set the PSO constants. - Max iteration=100, inertia weight damping ratio (W_d) =0.99, Swarm size=20, inetia weight w=1, learning coefficient ($c_1 = 2$, $c_2 = 2$). • Set constraint. - REF and LPSP • Set the research space: - lower and upper bounds for N_{PV} [0,100]. - lower and upper bounds for N_{WT} [0,50]. - lower and upper bounds for N_{BT} [0,100]. - lower and upper bounds for N_{AD} [0,3].
Step 3	Particles move to a new position based and update the iteration variable, inertia weight, velocity, and position
Step 4	Go back to step 2 and compute the objective functions.
Step 5	If satisfied stop otherwise go to steps 3 and 5
Step 6	If the best solution is obtained stop, if not repeat step 2

3.9.2 Cuckoo Search Algorithm

In the preceding chapter, the explanation of the CSA algorithm has been described. The progress of implementing the RB-EMS using the CSA as a benchmark method is demonstrated in Figure 3.18 by inserting load demand, objective functions (COE, LPSP, and REF), and economic and technical data for system components. Table 3.8 is given the steps of the CSA.

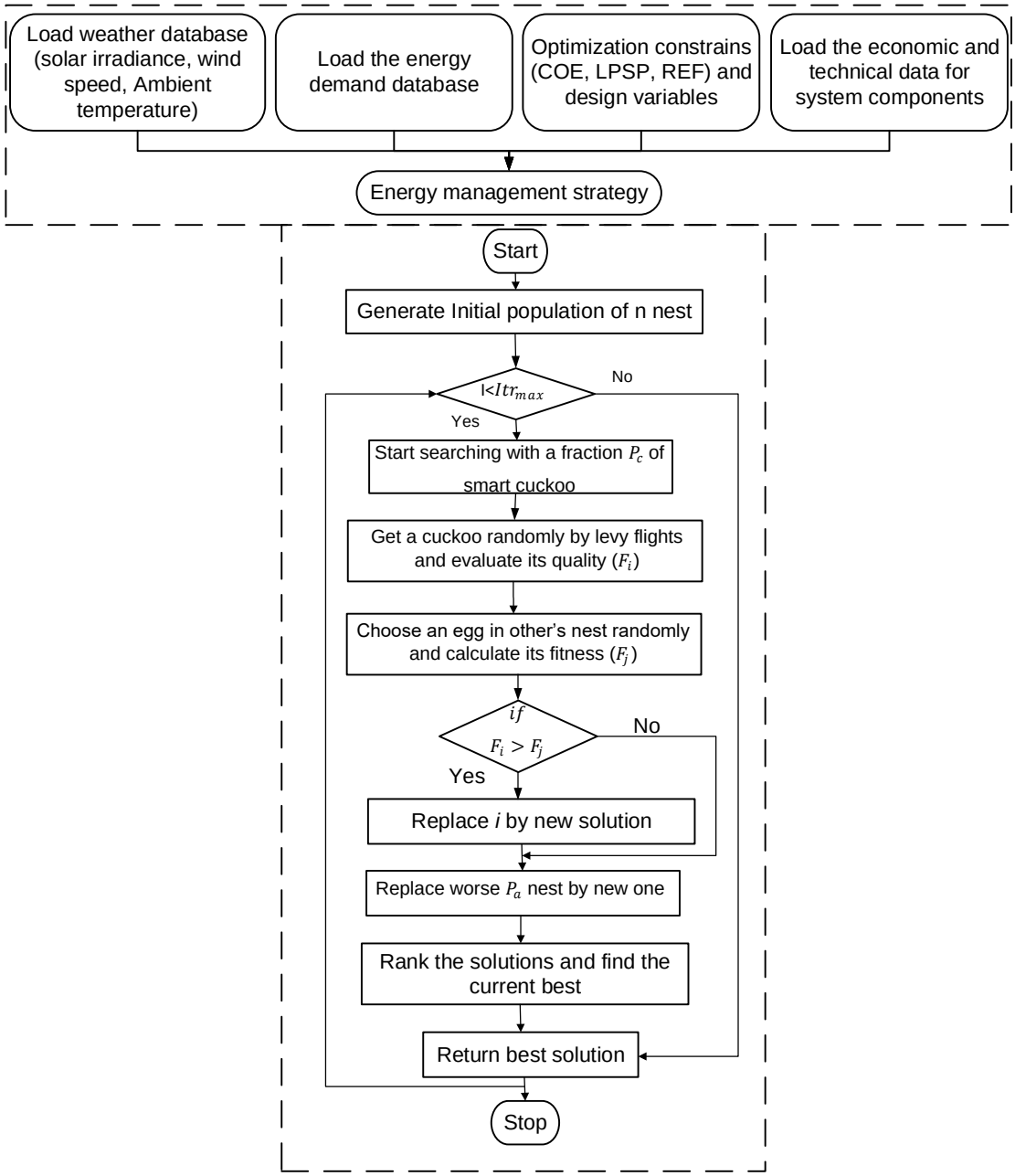

Figure 3.18 Flowchart of the Rule-Based-Energy Management Strategy of Cuckoo Search Algorithm.

Table 3.8 Steps of Cuckoo Search Algorithm.

Steps	Implementing operation
Step 1	• Loading weather database (Solar irradiance, Ambient temperature, Wind speed) is shown in Figures 4.2 (a), Figure 4.5 (a), and Figure 4.8 (a), respectively. • Load demand database figured in Figure 4.18 (c) • The load economic database for the microgrid components is listed in Table 3.3.
Step 2	• Set the CSA constants. - Abandoned nest fraction (P_a) =0.2, The fraction of the smart nest (P_c)=0.5, Nest number=5, Max iteration=100, • Set constraint. - REF and LPSP • Set the research space: - lower and upper bounds for N_{PV} [0,100] - lower and upper bounds for N_{WT} [0,50] - lower and upper bounds for N_{BT} [0,100]. - Lower and upper bounds for N_{AD} [0,3]
Step 3	Perform a local search around the population, evaluate the smart cuckoo, and update the best nest.
Step 4	Perform a global search through the lévy flight algorithm, evaluate the new nest, and update the best nest.
Step 5	Substitute fraction of worse nest P_a by new ones selected randomly, evaluate the new nests, and update the best nest.
Step 6	Update the optimum solution and increase the iteration variable
Step 7	If satisfied stop if not return to step 2.

The optimization control parameters for the utilized algorithms (IALO, ALO, PSO, CSA) are tabulated in Table 3.9 and were applied to obtain the presented result.

Table 3.9 The controlling parameters of the utilized optimization algorithms.

IALO & ALO algorithms [33]	CS algorithm [68]	PSO algorithm [94]
Search agents: 5	Number of the nest: 5	Swarm size: 5
Maximum iteration: 100	Maximum iteration: 100	Maximum iteration: 100
Best score: Elite antlion fitness	Fraction of abandoned nests (P_a) = 0.2	Initial weight (w): 1
Best position: Elite antlion position	Fraction of smart nest (P_c) = 0.5	Weighting factors (c_1 and c_2) = 2

3.10 Economic parameter analysis

The Stochastic Monte Carlo Method (SMCM) is a probabilistic numerical technique used to predict the result of a set of data and uncertain (stochastic) data. Furthermore, it is a stochastic tool developed by Neumann and Ulam and implemented in various fields to deal with the randomness of several components [180]. SMCM also known as multiple probability simulation named after a famous gambling city (Monaco-South France) involves large numbers of computer simulations with randomly selected input [43]. Furthermore, it is used when the input data is having complex or random variables such as charging and discharging different EVs for the long term [9]. The random prediction of the arrival and departure number of EVs along with the SMCM working principle is elaborated in the following subsection. This technique can be used to simulate situations that cannot be directly modeled.

Furthermore, the reason for utilizing stochastic methods is due to the goal of gaining information out of randomness. Besides, the popularity of the provided result from stochastic methods in the power system analysis and dealing with uncertain values. The characteristics of SMCM got attention among scholars due to its flexibility, runtime, and accuracy in solving a wide range of optimization problems in various fields [194]. Additionally, SMCM is due to the advantages such as providing multiple possible solutions from large random data [151]. On the contrary, the drawback of SMCM is acquiring different results in each run due to stochastic data [143]. In terms of applications, it is also applicated in project management, sciences, engineering, finance, and artificial intelligence [143]. The SMCM utilized an equation for the SoC_{EV} boundary is presented in Eq. (3.34). Furthermore, it is utilized to estimate the process of power flow and EV battery state (SoC) for charging and discharge the EVs for the period of one year [195]. The behavior of EVs is in uncertain number as proposed which ranging from 10 to 60 EVs. Moreover, it assesses the impact of an uncertain number of EVs on the grid.

$$SoC_{EVmin} < SoC_{EV} < SoC_{EVmax} \tag{3.34}$$

3.10.1 The working principle of the Stochastic Monte Carlo Method

SMCM principal work is involving the presented steps in Figure 3.19 after setting the period of time. The steps start with estimating the mathematical equation of system components to insert the output data, determine the needed values for analysis, and create a sample of random data for the SOC_{EVs}. Additionally, analyzing the acquired result followed by checking if the needed result was achieved as the maximum iteration number (17520 times) is reached, if yes, the program is stopped, otherwise go from the beginning to estimate the input data. Generally, in SMCM, the more random generated data, the better the estimated result**.**

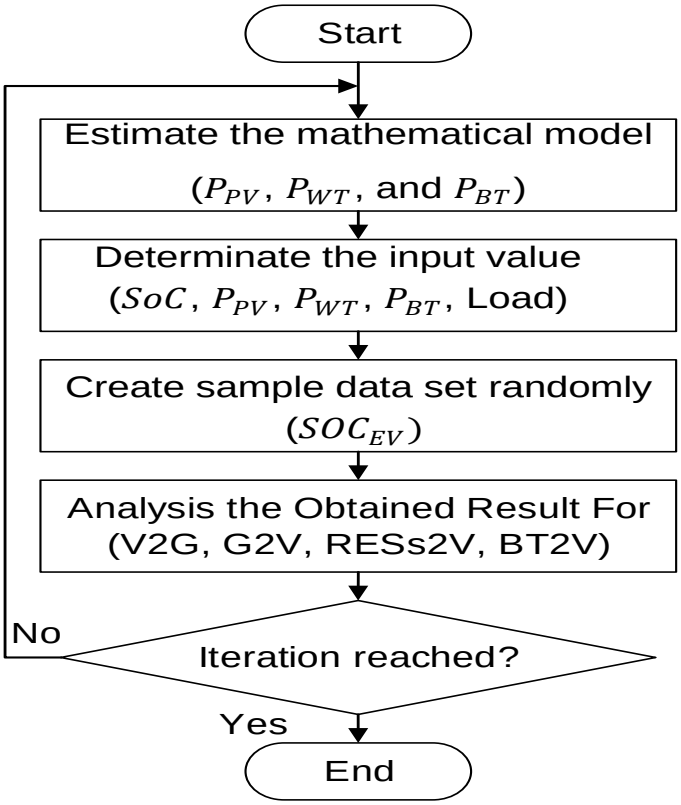

Figure 3.19 Flowchart of Stochastic Monte Carlo Method

3.10.2 Operational analysis of the Stochastic Monte Carlo Method

This section is customized for the implementation process of SMCM by creating uniform random (uniform distribution) data between 0 and 1 using Microsoft Office Excel to simulate the V2G and G2V outcomes. Furthermore, the impacts on

load, charging and discharging, amount of integrated energy from the RESs and grid, amount of exchanged energy from and to the EV (V2G and G2V), and BT2V are analyzed. The randomness of the SMCM is conserved to analyze the uncertain SoC_{EV} integrated with RES under a residential load.

The process starts by setting the types of data that will be processed with hourly data (8760) for a year as the flowchart presented in Figure 3.20. Then read the annual hourly data for (output power from the RESs (PV and WT), SOC_{EV} is randomly created, and Load demand data). Assuming during the simulation the RESs output power and load demand are constant values as obtained from the sizing method. After reading the data, defining the SOC_{EVmax} and SOC_{EVmin} boundaries, then, implementing uniform distribution operation into the V2G and G2V models to start running the data on the stochastic method. Uniform distribution describes the probability of random numbers for each EV. The size of SOC_{EV}-created data is (8760,1) utilized with yielded power from RESs and grid to meet the objective functions.

The SMCM is exploited due to the provided result and dealing with random variable data to gain results for uncertain situations. Besides, SMCM is utilized to evaluate the various scenarios for the uncertain behavior of EVs. The uncertain behavior refers to the SOC_{EV} battery by considering maximum and minimum SOC as 0.2% and 0.95%, respectively. The main considered scenarios for analysis with the help of SMCM in this study are Vehicle-to-Grid (V2G), Grid-to-Vehicle (G2V), Battery-to-Vehicle (BT2V), RESs2V, and the absence of EV (no EV). Besides, the aforementioned scenarios are analyzed when having a minimum (10) units, medium (30) units, and maximum (60) units of EVs.

In terms of implementation, the proposed scenarios of the case study on the built number of EVs that normally iterate during the year with 8760 hours are considered. While the stopping criteria for SMCM are considered till the highlighted scenarios are achieved. The simulation steps of SMCM were divided into an hourly basis for analyzing the impact of the EV under three scenarios as listed below to obtain a numerical result:

1. Setting the hourly data for the generated output power and load demand.

2. Define the initial SOC with SoC_{EVmin} (0.2%) and SoC_{EVmax} (0.95%) for the arrival and departure number of EVs randomly.

3. Creating hourly random SoC_{EV} data follows uniform distribution considering the scenarios ranges between 0-1 and sized (8760,1).

4. Acquiring the loads when SMCM converged, if yes ending the iteration, if not, return to step one as stopping criteria.

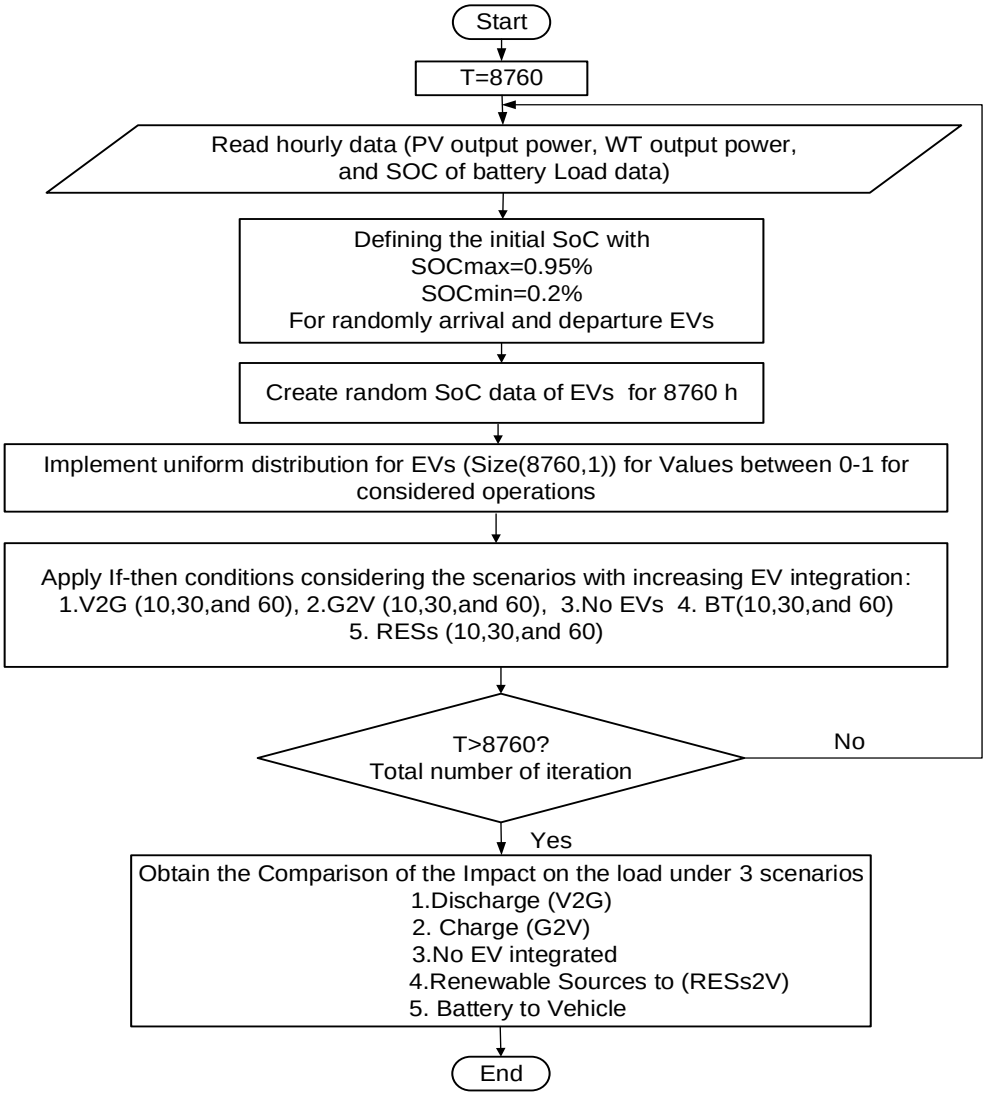

Figure 3.20 Flowchart of Stochastic Monte Carlo Method operation.

The operation of obtaining the result by conserving the case if the SoC_{EV} boundaries are carefully checked to get fully charged mode according to if-then conditions. The if-then condition of the operation of charging and discharging under various scenarios based on Eq. (3.34) is illustrated in Figure 3.21 as presented in Table 3.1. The obtained result from the presented operation is multiplied by the minimum (10), medium (30), and maximum (60) number of EVs to get the estimation of comparison of various scenarios.

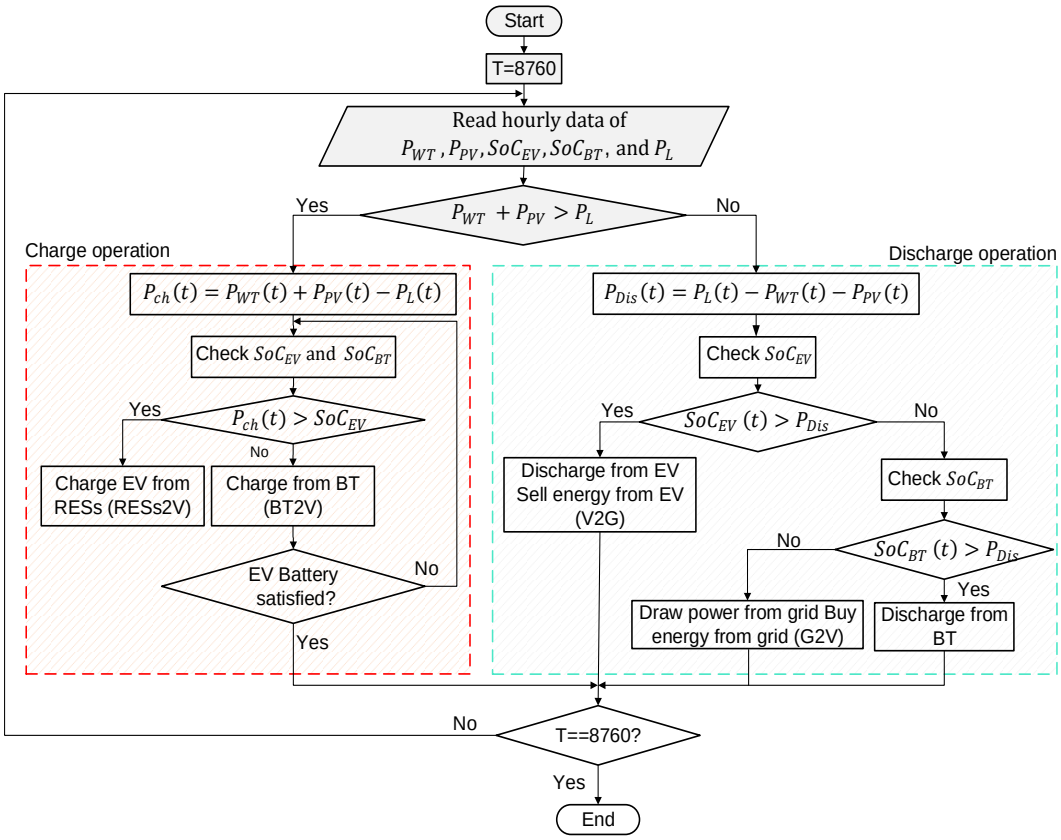

Figure 3.21 Operational strategies flowchart of IF-Then conditions for SMCM.

3.10.3 Arrival and departure time prediction

Based on SMCM as a valuable method for providing an accurate result, the implementation results with the help of mathematical equations will be presented [135][9]. The time prediction of arrival and departure EVs along with the SoC_{EV} are randomly acquired by Eq.(3.35)-Eq.(3.39). The considered charging power level for the charging home area is 11.5 kW which refers to level 2 and its efficiency is 86.5% [155].

$$T_{arrive}^{EV} \sim N\left(\mu_{EV_a}, \sigma_{EV_a}\right) \quad (3.35)$$

$$T_{Dep}^{EV} \sim N\left(\mu_{EV_d}, \sigma_{EV_d}\right) \quad (3.36)$$

$$SoC_{arrive}^{EV} \sim N\left(\mu_{EV_a}, \sigma_{EV_a}\right) \quad (3.37)$$

$$SoC_{Dep}^{EV} \geq 0.2 \times Cap_{EV} \quad (3.38)$$

$$SoC_{arrive}^{EV} < SoC_{Dep}^{EV} \quad (3.39)$$

where N is the normal distribution function depending on the mean (μ) and standard deviation (σ) for arrival (SoC_{arrive}^{EV}), departure time $\left(T_{Dep}^{EV}\right)$, and arrival ($T_{\text{arrive}}^{\text{EV}}$). Furthermore, departure (SoC_{Dep}^{EV}) is considered a constraint and the EV_d and EV_a are the departure and arrival vehicles. Additionally, between 12 pm - 24, am is the estimated arrival time while the departure estimated time is around 5 am-12 pm [9]. Besides, 0.2 represent the SoC_{EVmin} (0.2 %) of the EV battery and the Cap_{EV} is the EV battery capacity (from the manufacturer depending on the chosen EV) [9]. The listed data in Table 3.10 are utilized in order to estimate the arrival and departure times, and SoC_{EV}.

Table 3.10 The Entry constraints data of EV [8].

EV Constraints	Value	Unit
Maximum state of charge of EV (SoC_{max}^{EV})	0.95	%
Minimum state of charge of EV (SoC_{min}^{EV})	0.2	%
The mean of arrival EVs (μEVa)	18	-
Standards deviation of departure EV (σ_{EV_a})	2	-
The mean of departure EVs (μ_{EV_d})	7	-
Standards deviation of arrival EV (σ_{EV_d})	2	-
Electric Vehicle Capacity (Cap_{EV})	14	kWh
The arrival time of the EV $\left(T_{\text{arrive}}^{\text{EV}}\right)$	$12 \leq T_{arrive}^{EV} \leq 24$	h
The departure time of the EV $\left(Time_{Dep}^{EV}\right)$	$5 \leq Time_{Dep}^{EV} \leq 12$	h

3.10.4 Dynamic payback period analysis

To establish the project's financial profitability, economic research was undertaken based on the NPC and payback duration to show the break-even day [155]. Furthermore, the latter technique process is known as Discounted Payback Period (DPP) which was mathematically expressed in Eq. (3.40) with the help of Eq. (3.41) [196], [197]. The DPP refers to the number of years required to recover the initial investment in a project (free cash flow) [195]. The mathematical equation is used to calculate the NPC in order to gain better cost in comparison with the benchmarks using Discounted Cash Flow (DCF) analyses [184].

$$\text{DPP} = \sum_{t=0}^{DPP} S(1+ir)^{-t} - NPC_T = 0 \tag{3.40}$$

$$S = tariff \times (PL_{cumulative,sum} + EV_{demand}) \tag{3.41}$$

where S refers to the annual revenue generated by sold electricity to the consumers (EVs) as shown by Eq. (3.41) by assuming the residential tariff rate is \$0.05/kWh. The aforementioned tariff value multiplied by the residential suppled cumulative load ($PL_{cumulative,sum}$) in kW added to EV_{demand} to gain the total revenue which is measured in (\$/kWh). The ir represents the interest rate, $-t$ is the lifetime of the project, NPC_T denoted as Total Net Present Cost (TNPC) can be defined as the sum of the capital cost of components [108].

3.11 Chapter Summary

In this chapter, the methodology framework implemented in the study of the V2G integration system as a grid-connected system has been comprehensively elaborated. The explanation of the location of the case study, climatology conditions details, and energy demand data are described. The considered topology in this study is V2G for the proposed operation modes to charge and discharge EVs under residential load through a bidirectional AC/DC converter. Additionally, the RB-EMS

has been designed for power flow among the system components with the aid of four operation modes. Followed by the mathematical models equations of each component in the system used to obtain the individual yield of each component. The main three objective functions (COE, LPSP, and REF) have been discussed in detail with entry parameters for the utilized components. The aforementioned proposed objective functions of this study have been addressed by the proposed method IALO, while ALO, PSO, and CSA are chosen for benchmarking purposes and elaborated. An economic analysis method is considered to gain the DPP. Although a vast number of optimization algorithms are used to assess the behavior of the arrival and departure number of EVs, the Stochastic Monte Carlo Method is recommended due to its accuracy in providing outcomes. On the contrary, different optimized answers in each run. Chapter 4 details the full implementation of the raised issue related to V2G technology integration and its outcome.